3rd International Accelerator School for Linear Collider

Illinois, USA

LINAC-II

Lecture Notes

Oct. 22, 2008

Toshiyasu Higo

KEK

Contents of LINAC-II

6.2 Normal conducting TW detuned disk loaded structure

7. Ways to calculate HOM in cavity and cavities

7.1 Various ways of treating structure geometry

7.2 An detailed example: open mode expansion technique

8. Multi bunch beam dynamics and cures

8.1 Longitudinal of multi bunches

8.2 Transverse of multi bunches

8.3 Cure by damping modes

8.4 Cure by cancelling modes

8.5 Cure by hybrid scheme

9. Alignment of linac

9.1 One-to-one alignment

9.2 Dispersion free steering

9.3 Wakefield free steering

9.4 Alignment with using excited field in the accelerator structure

10. More issues for LC

10.1 Dark current capture

10.2 Tolerable trip rate

10.3 Summary of LINAC-II

Chapter 1 Realization of higher luminosity

1.1 Linac requirements for linear collider

The luminosity of the linear collider is the key parameter for the success of the experiment. It is expressed as,

$$L = \frac{f_{rep}\, n_b\, N^2\, H_D}{4\pi \sigma_x^* \sigma_y^*} \quad . \tag{1-1}$$

From this equation, we simply understand that the beam size σ_x and σ_y at the interaction point should be small with as large a bunch charge N as possible. If linac RF parameters allow, the number of collision should be maximized by increasing the number of bunches n_b in a pulse and repetition frequency f_{rep}.

In Lecture-I, we targeted higher energy,

$$e E_c = E_a L_{linac} = \frac{P_{linac}\, \eta_{RF->Beam}}{N N_b F_{rep}} \tag{1-2}$$

with increasing the efficiency from RF power to beam. The luminosity per unit power consumption for linac is expressed as,

$$\frac{L}{P_{linac}} = \frac{L_0 N_b F_{rep}}{e E_c N N_b F_{rep} / \eta_{RF->Beam}} = \frac{1}{e E_c} \frac{L_0}{N} \eta_{RF->Beam} \tag{1-3}$$

and it is found important also for luminosity to increase the power transfer efficiency. Here the L_0 is the luminosity expressed in eq. (1-1) and this is the main issue of this lecture-II. It is to be noted that the factor N^2 is included in L_0 so that the larger N gives higher luminosity in the scope of N dependence.

1.2 Cares to increase luminosity

Most important is to preserve through the linac the low emittance of the beam supplied from DR. This is the main issue of this lecture. Essentially, it is needed to preserve the 6 dimensional phase space of the beam. For the longitudinal emittance, the energy spread should be smaller than the acceptance of the final focus optics. For the transverse emittance, it is required to suppress the emittance growth within a tolerable level. The tolerable level is usually set such as a few tens of percent with respect to the one received from the DR.

1.3 Comparison of two LC parameters

The typical linac parameters of the two designs, ILC and CLIC, relevant to the present lecture are

listed for 500GeV c.m. energy case in the table of the following page. There are huge differences in acceleration RF related parameters and beam structure between the two cases, while the beam qualities such as emittances of the two cases are close. Following are some of the comparisons relevant to this lecture;

Beam emittance; comparable,
Beam current; ILC << CLIC by 100,
Number of bunches in a train; ILC > CLIC by 10,
Bunch spacing w.r.t. RF period; ILC >> CLIC by 100,
Bunch length; ILC >> CLIC by 10,
RF frequency; ILC < CLIC by 10,
Cavity aperture / wavelength; comparable

These parameters are closely related to the design of the linac and are described in the lecture.

One of the key differences is the bunch spacing shown in Fig. 1. In ILC, the spacing w.r.t. RF cycle is 468 while that of CLIC only 6. This means the damping requirement for the excited electromagnetic field is very stringent in CLIC.

The bunch length is ten times different. However, the ratio w.r.t. the RF frequency is similar so that the beam power spectrum in the unit of RF accelerating frequency is similar. In practice, as the bunch power spectrum at 10 times higher frequency than the accelerating mode is still more than 99% of the zero frequency one, it is high enough comparing to the frequency relevant to the component of the linac main parts. Therefore, all the modes and frequency components should be taken into account up the cutoff of the beam pipe and even considerably higher than it.

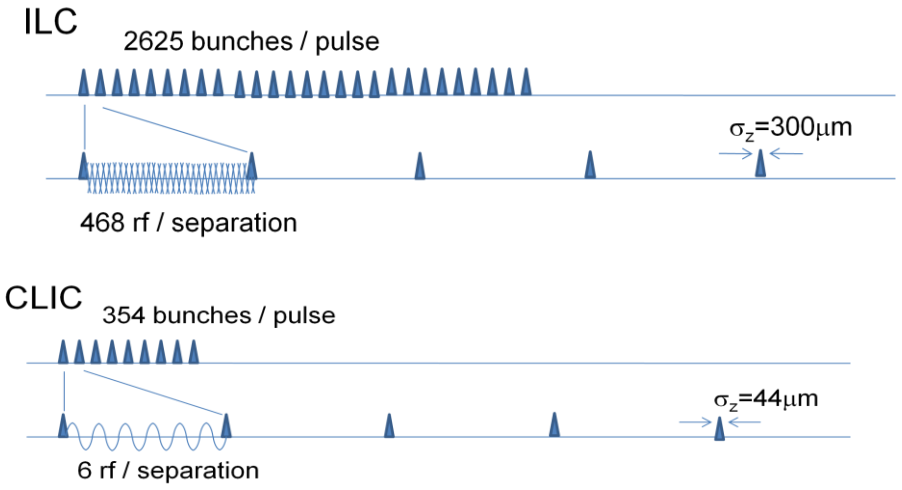

Fig. 1 Bunch parameters of two examples of linear collider linacs.

Table of relevant parameters of two LC design

Parameters		units	ILC(RDR)	CLIC(500)
Injection / final linac energy	E_{linac}	GeV	25 / 250	/ 250
Acceleration gradient	E_a	MV/m	31.5	80
Beam current	I_b	A	0.009	2.2
Peak RF power / cavity	P_{in}	MW	0.294	74
Initial / final horizontal emittance	ε_x	μm	8.4 / 9.4	2 / 3
Initial / final vertical emittance	ε_y	nm	24 / 34	10 / 40
RF pulse width	T_p	μs	1565	0.242
Repetition rate	F_{rep}	Hz	5	50
Number of particles in a bunch	N	10^9	20	6.8
Number of bunches / train	N_b		2625	354
Bunch spacing	T_b	ns	360	0.5
Bunch spacing per RF cycle	T_b / T_{RF}		468	6
Frequency	F	GHz	1.3	12
Beam phase w.r.t.RF		degree	5	15
EM mode in cavity			SW	TW
Number of cells in a cavity			9	19
Cavity beam aperture	a/λ		0.152	0.145
Bunch length	σ_z	mm	0.3	0.044

Chapter 2 Emittance dilution and preservation

2.1 Emittance preservation

Emittance preservation along the linac is one of the key issues of the main linac of LC. We should consider principally the 6-dimensional emittance. It is classified into two categories, the longitudinal emittance and the transverse one. The former is the energy and position along the bunch. The latter determine the transverse dimensions (x,y) while the derivative of these (x',y') are the phase space component. Present LC's are designed based on the large aspect ratio σ_x/σ_y, and it it usually treated somewhat independently, or in other words the coupling between the two directions is suppressed. Therefore, the phase spaces (x,x') and (y,y') are treated independently as long as the coupling between the two is kept small.

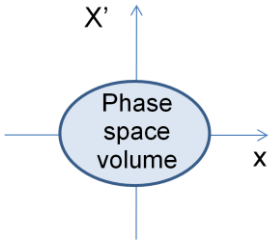

From another view point, the emittance is classified into two categories, single bunch emittance and multi bunch emittance. The former is the phase space occupied by a single bunch, while the latter the projection of all the bunched in a train. If it is not possible to correct the multi bunch phase space by any corrector, the projected emittance of the multi bunches is a measure to estimate the luminosity. In Fig. 2 are shown the dilution of single bunch emittance in three phases. The left is shown the negligibly small emittance, a point-like particle making a betatron oscillation along the ellipse. This can be corrected to zero if needed by simple corrector magnet. The center shows a coherent tail in the same bunch. Since this shape is still coherent along the bunch, it can be corrected by some mechanism depending on the position within a bunch. The right figure shows almost incoherent nature and the bunch fills whole phase space so that it cannot be corrected by any means once reached this phase.

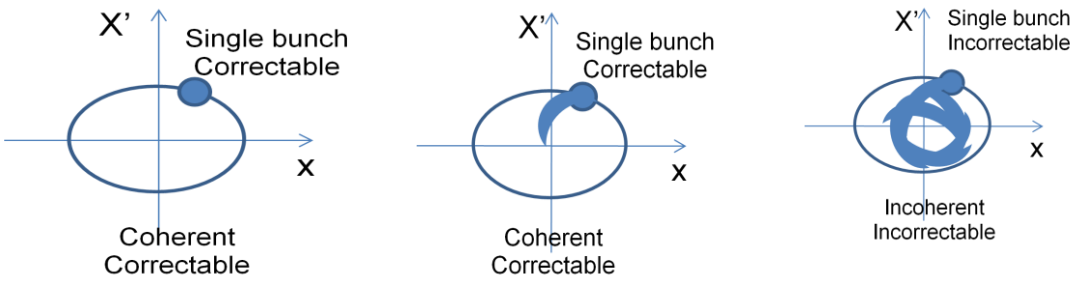

Fig. 2 Single bunch emittance and dilution.

In Fig. 3 are shown the projection of all the bunches in a multi-bunch emittance space. In the left figure is shown the case of all the bunches are moving in the same manner. In this ideal case, the multi bunch emittance is equal to that of the single bunch. In the center figure is shown the case with slowly varying phase space point. In this regime, each bunches can be corrected back to the nominal one by using a bunch-by-bunch fast corrector. If the dilution becomes to the right figure case, each bunch cannot be corrected anymore and the whole are in phase space becomes the measure for estimating the luminosity. The LC should not be operated in this regime.

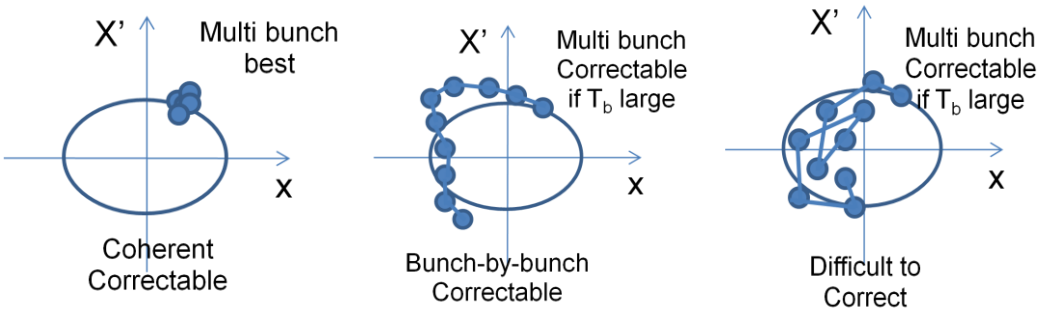

Fig. 3 Multi bunch emittance in phase space.

2.2 FODO optics and betatron oscillation

The transverse equation of motion is expressed as

$$\frac{d^2}{dz^2}x + k(z)x = 0 \qquad (2\text{-}1)$$

where

$$k(z) = \frac{c\,g}{E/e}[m^{-2}] \qquad (2\text{-}2)$$

,

where g is the field gradient of Q magnet, E electron beam energy, and c light velocity. The actual FODO optics is schematically shown in Fig. 4. By defining the parameters

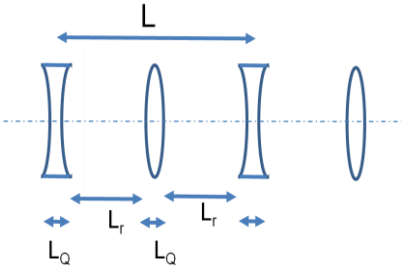

Fig. 4 FODO schematic.

$$\tau = \sqrt{k}\,L_r \quad \theta = \sqrt{k}\,L_Q,\ \eta = 2L_Q / L \qquad (2\text{-}3)$$

the transfer matrix connecting (x,x') from point 1 to point 2,

$$\begin{pmatrix} x \\ x' \end{pmatrix}_2 = (M)_{21} \cdot \begin{pmatrix} x \\ x' \end{pmatrix}_1 \qquad (2\text{-}4)$$

is given as below.

$$M_F = \begin{pmatrix} Cos\theta & \frac{1}{\sqrt{k}} Sin\theta \\ -\sqrt{k}\, Sin\theta & Cos\theta \end{pmatrix}, \quad M_D = \begin{pmatrix} Cosh\theta & \frac{1}{\sqrt{k}} Sinh\theta \\ -\sqrt{k}\, Sinh\theta & Cosh\theta \end{pmatrix} \tag{2-5}$$

Then the transfer matrix from the center of Q magnet to that of the next,

$$M_{FDF} = M_{F/2}\, M_{drift}\, M_D\, M_{drift}\, M_{F/2}$$

becomes

$$M_{FDF} = \begin{pmatrix} Cos\theta + \alpha\, Sin\mu & \beta\, Sin\mu \\ -\gamma\, Sin\mu & Cos\theta - \alpha\, Sin\mu \end{pmatrix} \tag{2-6}$$

with using Twiss parameters, (α, β, γ). In the thin lens approximation,

$$Cos\mu = 1 - \frac{\tau^2\theta^2}{2}, \; Sin\frac{\mu}{2} = \frac{\tau\theta}{2} = \frac{c\, g\, L^2}{8E/e}\eta(1-\eta) \tag{2-7}$$

And the actual oscillation along the linac, the betatron oscillation, is expressed as

$$x(z) \propto A\sqrt{\beta(s)}\; Sin(\psi(s) + \delta), \; \frac{d\psi}{ds} = \frac{1}{\beta(s)} \tag{2-8}$$

Let us assume $\beta(s)$ constant so that

$$x(z) \propto Sin(k_\beta\, s + \delta), \; k_\beta = \frac{1}{\beta(s)} = \frac{2\pi}{\lambda_\beta} \tag{2-9}$$

This becomes in the FODO lattice as

$$k_\beta = \frac{2\pi}{\lambda_\beta} = \frac{\mu}{L} = \frac{c\, g\, L}{4E/e}\eta(1-\eta) \;\; . \tag{2-10}$$

Here the betatron wavelength λ_β measures the wave length of the betatron oscillation along the linac. The μ is the phase advance per FODO cell. If we make the betatron wavelength constant along the linac, g should scale as E, energy, while in actual design it typically scales as square root of E.

It is the issue of this lecture to discuss the emittance dilution and preservation under the system guided by this kind of optical system.

2.3 Error sources for emittance dilution

It is important to suppress any sources of emittance dilution. There are many error sources which may increase the emittance.

If the optical parameters of the linac vary, they change the betatron phase/amplitude and makes the mismatch of the Twiss parameters at relevant position along the linac. This results in such as the dispersion leakage which makes the position variation of the bunch or bunch train depending on the energy spread. The transverse position may cause the emittance dilution.

If beam passed off axis w.r.t. Q magnets, it generates transverse kick and makes a dispersive effect within a bunch or among bunches in a train. To suppress this emittance growth, it is needed to measure the beam position and set it to adjust the alignment of the optical components or correct the beam to the optical system. To make the beam pass through the center of the Q-magnet, the beam position monitor BPM is usually set near the center of the Q-magnet.

The offset beam w.r.t. accelerating cavity generates the transverse wake field and this wake field affects the following particles, in the following bunches in a train or even the particles sitting in the same bunch but located at the later part. The wake field is also one of the critical issues to preserve the beam emittance, especially in a transverse phase space. The BPM plays an important role to adjust the beam position w.r.t. accelerating cavity. The cavity itself can function as BPM.

The acceleration is performed by RF field in cavities. If the amplitude or phase of this RF varies from bunch to bunch or within a train of bunches, it make the energy variation within a bunch or among bunches in a train. It also generates the transverse emittance dilution related to the dispersive mechanism. Therefore, RF stability is one of the key issues of the linac operation. The energy of the bunches in a train suffer from the longitudinal wake field produced by the precedent bunches. This is called as beam loading as for the accelerating mode view. This decrease of gain due to the beam itself can be compensated by feedback of RF field based on the measured cavity field, or adjusting the injection timing of the bunch trains w.r.t. RF field. The loading effect also exists within a bunch and it can be compensated by the phase of the RF w.r.t. beam. If not properly done, these errors result in the emittance through dispersive effect related to wake field.

If the accelerator cavity geometry has any asymmetry resulting in a field asymmetry, the variation of RF amplitude or phase also affects the beam energy gain depending on the position in a bunch. It may dilute the emittance through dispersive effect. The asymmetry comes from cavity tilt, asymmetry due to the coupler geometry, book shelf effect of the constituent cells not perpendicular to the axis of the structure, etc.

3. Wake field and impedance

The wake field and impedance is described in many text books[1]. This lecture covers some of the relevant results and some basic ideas for understanding.

3.1 Definition of wake function

The bunch of the high energy beam carries the electromagnetic field with Lorentz contraction as shown in Fig. 5. If such bunch passed through an aperture, the field is scattered and the resultant field exist around the obstacle as shown in Fig. 6. This field is called wake field.

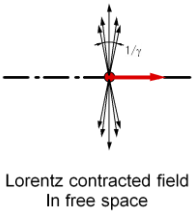

Fig. 5

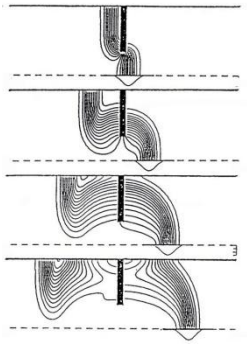

Fig. 6

The wake field is defined with a schematic description shown in Fig. 7. A bunch (red dot), with change q_1 with offset from the beam axis r_1, travels ahead of the following bunch (blue dot) with a separation of $s=ct$. Then the field experienced by the trailing particle integrated through the cavity or the structure is defined as the wake field. The following equation expressed this behavior[2].

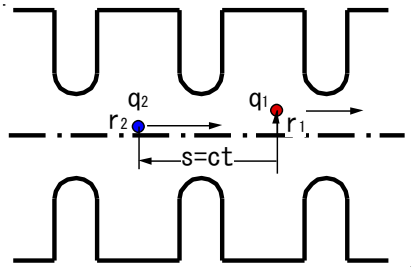

Fig. 7

$$W(r_1,s)=\frac{1}{q_1}\int_{-\infty}^{\infty}dz\left[E(r_1,z,t)+c\vec{z}\times B(r_1,z,t)\right]_{t=(s+z)/c}$$

$$\Delta p = q_1 q_2 W(s) \qquad (3\text{-}1)$$

where Δp is the momentum kick obtained by the following bunch. The kick in the beam direction is called the longitudinal wake field and defined as

$$W_L(r_1,s)=\frac{1}{q_1}\int_{-\infty}^{\infty}dz\left[E_z(r_1,z,t)\right]_{t=(s+z)/c} \qquad (3\text{-}2)$$

while that in the transverse direction is called the transverse wake field as expressed as

$$W_T(r_1,s)=\frac{1}{q_1}\int_{-\infty}^{\infty}dz\left[E(r_1,z,t)+c\vec{z}\times B(r_1,z,t)\right]_{T,t=(s+z)/c} . \qquad (3\text{-}3)$$

3.2 Panofsky Wenzel theorem

Let us derive one of the most basic features of the wake field relation called Panofsky Wenzel's theorem[3]. In order to make the derivation easy to understand, let us think about the transverse mode shown in Fig. 8. Here the mode consists of magnetic field H directing upward and the rotational electric field E around the H field. In this cross sectional view, the E field is in the beam direction.

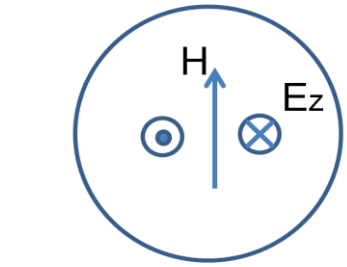

Think about TM11 field

$$\nabla \times E_z = -\frac{\partial}{\partial t} B_r$$

Fig. 8

From Maxwell's equation,

$$\vec{e}_z \times \nabla \times E = \vec{e}_z \times (-\frac{\partial B}{\partial t})$$

$$\therefore \vec{e}_z \frac{\partial B}{\partial t} = \vec{e}_\perp (\frac{\partial}{\partial z} E_\perp - \nabla_\perp E_z) \qquad (3\text{-}4)$$

If we use the relation

$$\frac{d}{dz} = \frac{\partial}{\partial z} + \frac{1}{c}\frac{\partial}{\partial t}$$

then the wake field given in (3-3) becomes

$$\frac{\partial}{\partial z} W_T(x,y,z) = \frac{1}{q_1}\int_{-\infty}^{\infty} dz \left[\frac{\partial}{\partial z} E_T + \vec{e}_z \times B\right] = -\frac{1}{q_1}\nabla_T \int_{-\infty}^{\infty} dz\, E_z \qquad (3\text{-}5)$$

Therefore,

$$\therefore \quad \frac{\partial}{\partial s} W_T = -\nabla_T W_L \quad , \qquad (3\text{-}6)$$

or in other way,

$$W_T(x,y,s) = -\nabla_T \int_{-\infty}^{s} ds' W_L(x,y,s') \quad . \qquad (3\text{-}6')$$

Using this relationship, we can estimate transverse wake field from the longitudinal wake field. In other words, the transverse wake field relates to the longitudinal one through this equation. This is how the beam interacts with the transverse wake field if it passed off axis and no wake field if passed on axis where no E_z field exists, such as shown in the dipole more field in a pillbox described in Lecture-I.

3.3 Multipole expansion

From Panofsky Wenzel theorem,

$$W_L = -\frac{\partial}{\partial s} W, \quad W_T = \nabla_T W \tag{3-7}$$

For axisymmetric environments, these W can be expanded into multi-poles,

$$W(r, r', \theta, s) = \sum_{m=0}^{\infty} W_m(r, r', s) Cos(m\theta) \tag{3-8}$$

From Maxwell's equation, form of W_m can be found,

$$W_m(r, r', s) = F_m(s)\, r^m\, r'^m \tag{3-9}$$

so the wake functions are now expressed as,

$$\begin{aligned} W_L^{(m)}(r, r', s) &= \frac{\partial}{\partial s} F_m(s)\, r^m\, r'^m\, Cos(m\theta) \\ W_T^{(m)}(r, r', s) &= m\, F_m(s)\, r^{m-1}\, r'^m [\vec{r}\, Cos(m\theta) - \vec{\theta}\, Sin(m\theta)] \end{aligned} \tag{3-10}$$

From these we understand that the wake field near axis exists only m=0 term for longitudinal wake and m=1 term for transverse wake. The former is constant over radius, while the latter linear over drive bunch offset but constant on witness bunch position.

3.4 Impedance

The impedance is defined as the Fourier transform of the wake function as below.

$$Z_L(x, y, \omega) = \int_{-\infty}^{\infty} d(\frac{s}{c}) W_L(x, y, s)\, e^{-j\omega\frac{s}{c}} \tag{3-11}$$

$$Z_T(x, y, \omega) = -j \int_{-\infty}^{\infty} d(\frac{s}{c}) W_T(x, y, s)\, e^{-j\omega\frac{s}{c}} \tag{3-12}$$

Panofsky Wenzel theorem becomes

$$\frac{\omega}{c} Z_T(x, y, \omega) = \nabla_T\, Z_L(x, y, \omega) \tag{3-13}$$

Since the physical wake field is real, the impedance has the following symmetry.

$$\mathrm{Re}\{Z_L(\omega)\} = \mathrm{Re}\{Z_L(-\omega)\}, \quad \mathrm{Im}\{Z_L(\omega)\} = -\mathrm{Im}\{Z_L(-\omega)\} \tag{3-14}$$

Therefore,

$$W_L(s)=\frac{1}{2\pi}\int_{-\infty}^{\infty}d\omega Z_L(\omega)e^{j\omega\frac{s}{c}} \\ =\frac{1}{2\pi}\int_{-\infty}^{\infty}d\omega[\{\mathrm{Re}\{Z_L(\omega)\}Cos(\omega\frac{s}{c})-\mathrm{Im}\{Z_L(\omega)Sin(\omega\frac{s}{c})\}] \tag{3-15}$$

Moreover from causality,

$$W_L(-s)\}=0 \ \ for\ all\ s>0 \\ \therefore\int_{-\infty}^{\infty}d\omega\,\mathrm{Re}\{Z_L(\omega)\}Cos(\omega\frac{s}{c})=-\int_{-\infty}^{\infty}d\omega\,\mathrm{Im}\{Z_L(\omega)\}Sin(\omega\frac{s}{c}) \tag{3-16}$$

These are some of the impedance characteristics. Finally, wake function is calculated from only the real part of the impedance,

$$W_L(s)=\frac{1}{\pi}\int_{-\infty}^{\infty}d\omega\{\mathrm{Re}\{Z_L(\omega)\}Cos(\omega\frac{s}{c}) \tag{3-17}$$

Actual real part of the impedance is illustrated as shown in Fig. 6. Here each resonance is expressed as

$$Z_L(\omega)=\frac{R}{1+jQ(\frac{\omega}{\omega_0}-\frac{\omega_0}{\omega})}$$

where the ω_0 is the resonant frequency of the mode. At low frequency region, there are isolated trapped modes. Above the cutoff off frequency of the beam pipe, the power escapes into the beam pipe and the resonances are not isolated but overlapped and show almost continuous behavior.

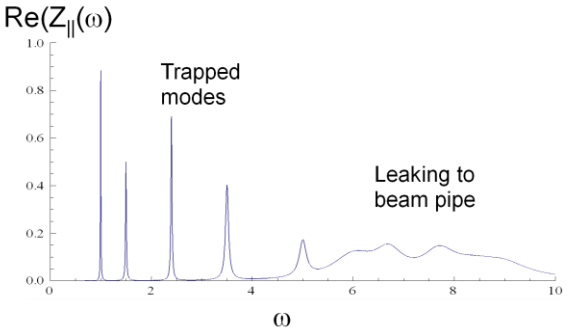

Fig. 9 Schematic of real part of impedance.

To estimate the wake field for those isolated modes, the representation of the resonant mode is useful. For higher frequency case, it is convenient to deal with the wake function directly.

3.5 Loss parameter

The electric field and the voltage across a cavity are expanded into a series of modes.

$$E_z(\vec{r},t)=\mathrm{Re}\{\sum_{n=0}^{\infty}E_n(\vec{r})e^{j\omega_n t}\} \\ V_n=\int_{-\infty}^{\infty}dz\,E_{z,n}(\vec{r})e^{j\omega_n\frac{z}{c}} \tag{3-18}$$

Here we define the loss parameter. In SW cavity case, it is expressed

$$k_n = \frac{|V_n|^2}{4U_n} \qquad \text{Per a cavity} \tag{3-19}$$

$$k_n = \frac{|E_n|^2}{4u_n} \qquad \text{per unit length} \tag{3-20}$$

where V_n represents the voltage across the cavity and U_n the stored energy in the cavity, while E_n the electric field and u_n the stored energy per unit length. For delta-function like point driving particle,

$$W_L^{\delta}(s) = \sum_{n=0}^{\infty} 2k_n \, Cos(\omega_n \frac{s}{c}) \tag{3-21}$$

Since the self wake is half of the wake behind the bunch, the energy lost in mode *n* is expressed as

$$\Delta U_n = k_n \, q_1^2 \tag{3-22}$$

For finite bunch length, simply multiply the bunch form factor as

$$\rho(\vec{r},t) = q_1 \, \lambda(z-ct),$$
$$\lambda(s) = \frac{1}{\sqrt{2\pi}} \exp\{-\frac{(s-s_0)^2}{2\sigma_z^2}\} \tag{3-23}$$

And the actual wake is the following convolution

$$W_L(s) = \int_0^{\infty} ds' \, \lambda(s-s') \, W_L^{\delta}(s') \tag{3-24}$$

Loss to such as the fundamental mode becomes

$$k_{fund} = k_0 \exp\{-\frac{1}{2}(\frac{\omega}{c})^2 \sigma_z^2\} \tag{3-25}$$

That for higher modes is similarly

$$k_{HOM} = \sum_{n=1}^{\infty} 2k_n \exp\{-\frac{1}{2}(\frac{\omega_n}{c})^2 \sigma_z^2\} \tag{3-26}$$

This estimates all the energy lost in passing a cavity on axis, except for the fundamental one.

3.6 Longitudinal wake function

If we perform the summation up to some finite number of modes

$$W_L^{\delta}(s) = \sum_{n=0}^{N} 2k_n \, Cos(\omega_n \frac{s}{c}) \tag{3-27}$$

We get the wake function as shown in Fig. 10 taken from the Lecture note[4]. This is the estimation of SLAC disk loaded accelerator structure geometry. The functional shape should be scaled to any frequency as long as the geometry is scaled proportionally. The contribution of those higher than the frequency, and in high energy limit $\gamma >> \omega a/c$, the optical resonator model predicts[5] the functional form as

$$k_n \equiv \frac{E_{0n}^2}{4u_n}, \quad and \quad u_n = k_n (\frac{r_q}{a})^{2m} q^2 \qquad . \tag{3-28}$$

Adding this contribution makes the estimation of very short range wake field as shown with solid line in the figure. In much longer time scale, the contribution from the accelerating mode dominates, because of the cancellation of higher modes. This is shown in the lower figure of Fig. 10.

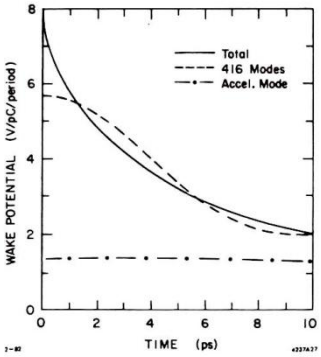

Fig. 9.3. Longitudinal wake per cell for the SLAC disk-loaded structure (0-10 ps). Cell length = 3.5 cm; beam aperture radius = 1.163 cm.

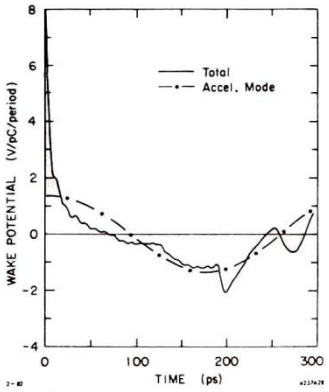

Fig. 9.4. Longitudinal wake per cell for the SLAC disk-loaded structure (0-300 ps).

Fig. 10

3.7 Transverse wake function

Consider a periodic disk-loaded structure with beam hole aperture radius a. The synchronous space harmonic component of the n-th TW mode, axial electric field is expressed as[6]

$$E_{zn} = E_{0n} (\frac{r}{a})^m \, Cos(m\phi) \, Cos\{\omega_n (t - z/c)\} \tag{3-29}$$

where E_{0n} is the field at r=a. On the other hand the loss parameter is expressed as

$$k_n \equiv \frac{E_{0n}^2}{4u_n}, \quad and \quad u_n = k_n (\frac{r_q}{a})^{2m} q^2 \tag{3-30}$$

where r_q is the offset of drive bunch. Therefore,

$$\therefore \quad E_{0n} = -2(\frac{r_q}{a})^m k_n \, q \tag{3-31}$$

With q the witness bunch charge. Then the wake function can be expressed as

$$\therefore \quad E_{zn} = -2k_n q\left(\frac{r}{a}\right)^m \left(\frac{r_q}{a}\right)^m Cos(m\phi) Cos(\omega_n \frac{z}{c}) \tag{3-32}$$

If we take Panofsky Wenzel theorem

$$(E_T + c B_T)^{(cmf)} = j(c/\omega)\nabla_T E_z^{(cmf)} \tag{3-33}$$

The transverse wake field becomes as

$$W_{Tn}(\tau) = 2\left(\frac{k_n c}{\omega_n a}\right)\left(\frac{r_q}{a}\right) Sin(\omega_n \tau) \tag{3-34}$$

So the following summation

$$W_T(\tau) = 2\left(\frac{r_q}{a}\right)\sum_n \left(\frac{k_n c}{\omega_n a}\right) Sin(\omega_n \tau) \tag{3-35}$$

gives the total transverse wake field. Over the maximum frequency ω_m, integration gives wake field using

$$\frac{dk}{d\omega} = \frac{A_1}{\omega^{3/2}} \tag{3-36}$$

The actually calculated wake field for SLAC disk-loaded structure are shown in three time ranges, taken from P. Wilson's Lecture Note[4].

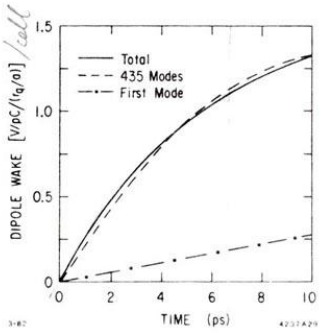

Fig. 9.5. Dipole wake per cell for the SLAC disk-loaded structure (0-10 ps).

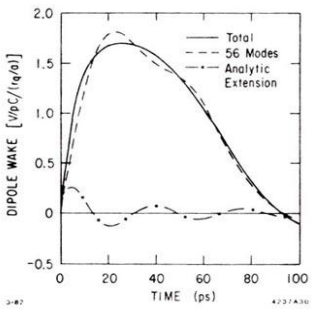

Fig. 9.6. Dipole wake per cell for the SLAC disk-loaded structure (0-100 ps).

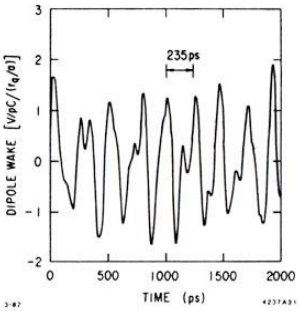

Fig. 9.7. Dipole wake per cell for the SLAC disk-loaded structure (0-2000 ps).

Fig. 11 Transverse wake field calculated for SLAC disk loaded structure. Taken form P. Wilson's Lecture note.

From these figures in Fig. 11, we see that the initial slope is linear, where the fundamental mode contribution is very small. The initial bump is determined by about 50 modes. Much longer time range, the lowest dominant mode dominates and it is clearly seen at about 4 GHz.

The transverse wake function is calculated and parametrized in (a,g,L) parameters by K. Bane[7]. Here, the parameters are a=beam hoe aperture, L=cell length and g=L-t, where t=disk thickness. The calculation was performed in the X-band linear collider range for NLC, where

$0.35 < a/L < 0.7$

$0.55 < g/L < 0.9$

The obtained formula is

$$W_T(s) = \frac{4Z_0 c s_0}{\pi a^4} \{1-(1+\sqrt{s/s_0})\, Exp(-\sqrt{s/s_0})\} \qquad (3\text{-}37)$$

where Z0 is wave impedance in free space, and $0 < s < 0.15$ L is the special separation of the witness particle behind the driving one. S0 is given from fitting the calculations of the parameter space and gives as

$$Z_0 = 377\,\Omega, \quad s_0 = 0.169\, \frac{a^{1.79} g^{0.38}}{L^{1.17}} \qquad (3\text{-}38)$$

The typical examples are shown in Fig. 12. The red, green and blue curves corresonds to the wake field of the cases with a=3mm, 4mm and 5mm. Here the L=9mm and g=7mm in all cases.

In this figure, strong a dependence is clearly shown in addition to the initial linear slope. The initial slope is given by differentiating eq. (3-37) as

$$\frac{\partial}{\partial s} W_T(s) = \frac{2 Z_0 c}{\pi a^4} \qquad (3\text{-}39)$$

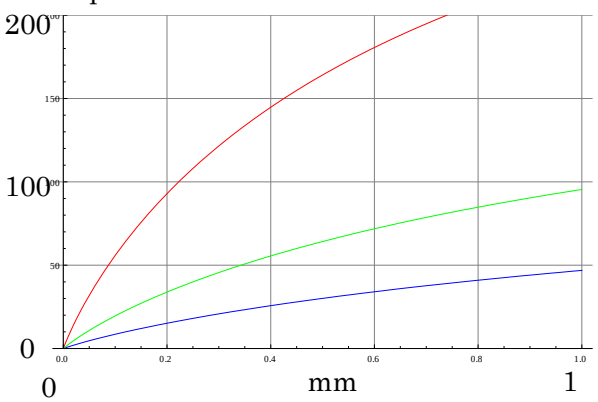

Fig. 12 Transverse wake function of X-band structure using the formula by K. Bane.

And this slope becomes an important parameters describing the transverse wake field for the beam dynamics problems.

4. Single-bunch beam dynamics and cures against emittance dilutions

4.1 Beam dynamics under shot range transverse wake field

Newton's equation of motion in a transverse plane is expressed by

$$F_x = \frac{dp_x}{dt} = \frac{d}{dt}\gamma m_0 \frac{dx}{dt} = m_0 c^2 \frac{d}{ds}\gamma \frac{dx}{ds} \quad , \tag{4-1}$$

where F_x is the transverse force experienced by the bunch in the transverse direction x. The s is the longitudinal coordinate and for the particle travelling with the velocity of light, it is $s=ct$. The γ is the Lorentz factor of the particle and m_0 the electron rest mass.

Consider a bunch with its center at s along the linac. The transverse position of the particles inside the bunch is expressed as $x(s,z)$, where z is measured from the bunch center. Under the force due to the transverse wake field, the equation of motion becomes

$$m_0 c^2 \frac{d}{ds}\gamma \frac{d}{ds} x(s,z) + m_0 c^2 k_\beta^2 x(s,z) = e\,Ne \int_z^\infty dy\, x(s,y)\, w(y-z)\, \lambda(y) \quad , \tag{4-2}$$

where the charge distribution of the bunch is expressed as $\lambda(y)$ and the wake field by $w(y-z)$, where the wake field for a particle at z due to the driving charge at y is expressed as a function of the mutual distance, y-z. The second term of the left hand side is the focusing term by the linac optical elements. Then, the equation (4-2) becomes

$$\frac{1}{\gamma}\frac{d}{ds}\gamma \frac{d}{ds} x(s,z) + k_\beta^2 x(s,z) = \frac{N r_e 4\pi\varepsilon_0}{\gamma} \int_z^\infty dy\, x(s,y)\, w(y-z)\, \lambda(y) \tag{4-3}$$

where $r_e = \frac{1}{4\pi\varepsilon_0}\frac{e^2}{m_0 c^2}$ is the classical electron radius.

4.2 Two particle model

Without acceleration, the equation (4-3) becomes

$$\frac{d^2}{ds^2} x(s,z) + k_\beta^2 x(s,z) = \frac{N r_e 4\pi\varepsilon_0}{\gamma} \int_z^\infty dy\, x(s,y)\, w(y-z)\, \lambda(y) \tag{4-4}$$

Let us assume that the bunch is divided into head and tail with each containing a charge of $Ne/2$ separated by $2\sigma_z$. Since there is no wake field for the head particle, the transverse motion of the head x_1 is expressed as

$$x_1(s) = \hat{x}_1 \, Cos\, k_\beta s \tag{4-5}$$

The field seen by the tail particle F2 is expressed as

$$F_2 = e\frac{N e}{2} x_1 w(2\sigma_z) \tag{4-6}$$

So that the equation becomes

$$y(s) = -\frac{j x_1}{2 k_\beta} s \quad . \tag{4-7}$$

This is a forced oscillation with the same frequency as the betatron oscillation. This can easily be solved with the functional form

(4-8)

,

where the y(s) is a slowly varying function with respect to the betatron oscillation with the wave length $2\pi/k_\beta$. Here the equation for the y(s) is

$$y''(s) + 2 j k_\beta y'(s) = \hat{x}_1 \tag{4-9}$$

with a solution

$$y(s) = -\frac{j \hat{x}_1}{2 k_\beta} s \tag{4-10}$$

saying that the tail oscillates at a phase $\pi/2$ behind. The tail amplitude linearly increases as the position *s* in the linac.

4.3 Chao-Richter-Yao estimation

A little more sophisticated estimation was performed by Cho-Richter-Yao[8]. Starting with the equation (4-4) in a general bunch shape and setting the initial condition as

$$x(0,z) = x_0 \quad , \quad \left.\frac{\partial x}{\partial s}\right|_{s=0} = 0 \quad , \tag{4-11}$$

in a weak wake field condition

$$\frac{N r_e w}{\gamma} << k_\beta^2 \tag{4-12}$$

we can solve the equation with the expression as

$$x(s,z) = a(s,z) e^{j k_\beta s} \tag{4-13}$$

,

where *a(s,z)* is a slowly varying function. Inserting this into the eq. (4-4), we get the equation of

a(s,z) as

$$\frac{\partial a}{\partial s} = -j\frac{N r_e}{2 k_\beta \gamma}\int_z^\infty dy\, a(s,y)\, w(y-z)\,\lambda(y) \tag{4-14}$$

Let us define the wake field as

$$w = w' z \ , \ and \quad \lambda(z) = 1/2l_b \tag{4-15}$$

Then the equation of motion becomes

$$\frac{\partial a}{\partial s} = -j r\int_z^\infty dy (y-z)\, a(s,y) \tag{4-16}$$

with a parameter

$$r = \frac{N r_e w'}{2 k_\beta \gamma l_b} \quad . \tag{4-17}$$

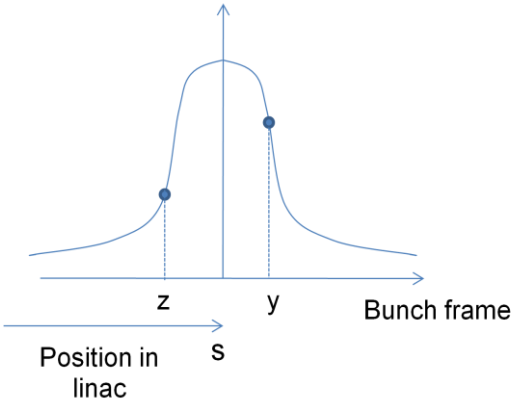

Fig. 12 Bunch shape and related coordinates.

It has an asymptotic solution as[8]

$$a = \frac{x_0}{\sqrt{6\pi}}(2 r s z^2)^{-1/6}\, Exp[\frac{3^{3/2}}{4}(2 r s z^2)^{1/3}] \quad . \tag{4-18}$$

When we take the acceleration into account, we take back to the equation (4-3). We assume slow acceleration,

$$\gamma'/\gamma << k_\beta \quad or \quad \frac{d\gamma}{ds}\frac{\lambda_\beta}{2\pi} << \gamma \tag{4-19}$$

We start with the case of no wake field. In this case,

$$\frac{d^2}{ds^2}x + \frac{\gamma'}{\gamma}\frac{d}{ds}x + k_\beta^2 x = 0 \tag{4-20}$$

Again we take the functional form (4-13) and the equation becomes

$$2\frac{\partial a}{\partial s} + \frac{\gamma'}{\gamma}a = 0 \tag{4-21}$$

And this has a solution

$$a(s,z) = a_0(z)\sqrt{\gamma_0/\gamma(s)} \tag{4-22}$$

This is equivalent to the adiabatic damping due to the acceleration in z-direction. Now let the wake field ON. The equation (4-3) becomes

$$2\,jk_\beta\,\frac{\partial a}{\partial s}+\frac{\gamma'}{\gamma}\,jk_\beta\,a=\frac{N r_e 4\pi\varepsilon_0}{\gamma}\int_z^\infty dy\,a(s,y)\,w(y-z)\,\lambda(y) \tag{4-23}$$

Let us define now

$$a(s,z)=b(s,z)/\sqrt{\gamma(s)} \tag{4-24}$$

So that the equation of *a(s,y)* becomes that of *b(s,y)* as

$$\frac{\partial b}{\partial s}=-j\frac{N r_e 4\pi\varepsilon_0}{2k_\beta\gamma(s)}\int_z^\infty dy\,b(s,y)\,w(y-z)\,\lambda(y) \tag{4-25}$$

This is exactly the same form as the equation for *a(s,y)* in (4-14) except for the varying $\gamma(s)$ here. If we further take the coordinate *s* replaced by *S* as below,

$$dS=ds/\gamma(s) \tag{4-26}$$

The equation becomes finally

$$\frac{\partial b}{\partial S}=-j\frac{N r_e 4\pi\varepsilon_0}{2k_\beta}\int_z^\infty dy\,b(s,y)\,w(y-z)\,\lambda(y) \tag{4-27}$$

Which is now exactly the same form as *a(s,z)* in (4-14). Therefore, we get the same solution in its asymptotic form. Consider a constant acceleration,

$$\gamma(s)=\gamma_i+s(\gamma_f-\gamma_i)/L \tag{4-28}$$

Then *S* becomes

$$S=\frac{L}{\gamma_f-\gamma_i}\ln\frac{\gamma(s)}{\gamma_i}\approx\frac{L}{\gamma_f}\ln\frac{\gamma(s)}{\gamma_i} \tag{4-29}$$

And the solution is expressed as

$$b=\frac{x_0}{\sqrt{6\pi}}(2r\,S\,z^2)^{-1/6}\,Exp[\frac{3^{3/2}}{4}(2r\,S\,z^2)^{1/3}]\quad where\ r=\frac{N r_e 4\pi\varepsilon_0 w'}{2k_\beta l_b} \tag{4-30}$$

Note that the parameter r is now a little different from (4-17). Since S_{final} is expressed as

$$S_{final}\approx\frac{L}{\gamma_f}\ln\frac{\gamma_f}{\gamma_i}=L/\gamma_{eff}\quad where\ \gamma_{eff}=\gamma_f/\ln\frac{\gamma_f}{\gamma_i} \tag{4-31}$$

And the actual amplitude *a(s,z)* is expressed as

$$a=\frac{1}{\sqrt{\gamma(s)}}\frac{x_0}{\sqrt{6\pi}}(2r\,S\,z^2)^{-1/6}\,Exp[\frac{3^{3/2}}{4}(2r\,S\,z^2)^{1/3}] \quad where \quad r=\frac{N\,r_e\,4\pi\,\varepsilon_0\,w'}{2k_\beta\,l_b} \tag{4-32}$$

The functional form is shown in Fig. 14.

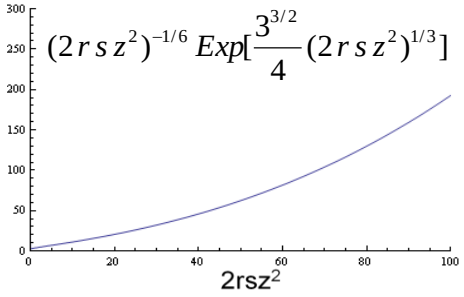

Fig. 14 Asymptotic form.

4.4 BNS damping

Let us start with two particle model form.

$$\frac{d^2}{ds^2}x_2+k_\beta^2\,x_2=-\frac{N\,r_e\,4\pi\,\varepsilon_0\,w(2\sigma_z)\,x_1}{2\gamma}=-C\,\hat{x}_1\,e^{j\,k_\beta\,s} \tag{4-33}$$

If we can vary the tail particle oscillation frequency from that of the head particle as below,

$$\frac{d^2}{ds^2}x_2+(k_\beta^2+\Delta k_\beta^2)\,x_2=-\frac{N\,r_e\,4\pi\,\varepsilon_0\,w(2\sigma_z)\,x_1}{2\gamma}=-C\,\hat{x}_1\,e^{j\,k_\beta\,s} \tag{4-34}$$

the resonant growth of the second particle should be suppressed. From FODO lattice, the phase advance per cell is expressed as (2-7) so that if varies the beam energy δ, the phase advance varies

$$\frac{1}{2}Cos\frac{\mu}{2}\frac{d\mu}{d\delta}=\frac{c\,g\,L^2}{8E^2/e}\eta(1-\eta)$$

so that

$$\frac{d\mu}{d\delta}=-2Tan\frac{\mu}{2} \quad . \tag{4-35}$$

The energy variation within a bunch results in the variation of k_β as

$$\frac{dk_\beta}{d\delta}=\frac{1}{L}\frac{d\mu}{d\delta}=-\frac{2}{L}\tan\frac{\mu}{2} \tag{4-36}$$

This suppression mechanism is called BNS damping[9].

In practice, the energy tapering to make the larger focusing force for tail particle can be done with lowering the energy toward the tail. It can be produced by setting the bunch in RF slope toward the decreasing slope. The longitudinal wake function naturally helps decreased the energy toward the tail.

4.5 Auto phasing

We start with the equation of motion with focusing force variation along the bunch.

$$\frac{d^2}{ds^2}x(s,z)+\{k_\beta^2\,x(s,z)+\Delta k_\beta^2\,x(s,z)\}=\frac{N\,r_e\,4\pi\,\varepsilon_0}{\gamma}\int_z^\infty dy\,x(s,y)\,w(y-z)\,\lambda(y) \quad (4\text{-}37)$$

If we can vary the focusing force as

$$\Delta k_\beta^2(s,z)=\frac{N\,r_e\,4\pi\,\varepsilon_0}{\gamma}\int_z^\infty dy\;w(y-z)\,\lambda(y) \quad (4\text{-}38)$$

then the solution becomes simply

$$x(s,z)=x(s)=x_0\cos(k_\beta\,s) \quad (4\text{-}39)$$

This is stable and x(s) does not depend on z, which means the both head and tail oscillate staying at the same oscillation phase as shown in Fig. 15.

This suppression scheme is called autophasing. The slope on k_β is produced by energy profile inside the bunch with amplitude of the order of

$$\Delta k_\beta^2\approx\frac{N\,r_e\,4\pi\,\varepsilon_0\,W_\perp'(2\sigma_z)}{\gamma} \quad (4\text{-}40)$$

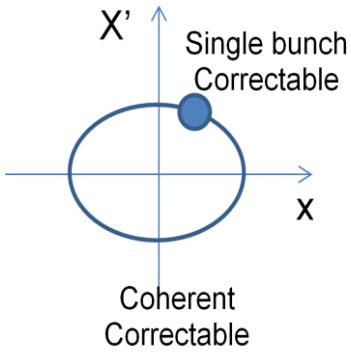

Fig. 15

The big energy slope needed for this compensation should be compensated at the downstream of linac where the beam is stable with higher energy.

5. Long range wake field

5.1 Fundamental theorem of beam loading

Assume a cavity field in phasor diagram focusing on one dominant mode as shown in Fig. 16. The vector representing cavity field rotates at an angular velocity ω, while the reference frame can be set at any definition. We define here with the beam arrival time to be θ=0 as shown in Fig. 17. The beam excited field if V_b, which is different from the pure decelerating field V_e by an angle ε. When the second bunch enters into the same cavity, the phasor relation becomes as in Fig. 18.

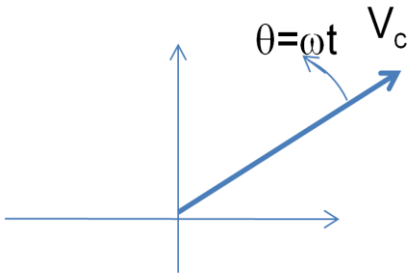

Fig. 16 Phaser representation

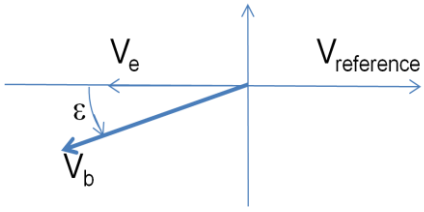

Fig. 17 Beam excited field at the injection of the first bunch into an empty cavity.

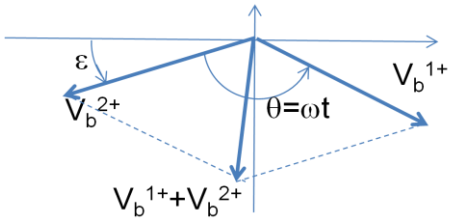

Fig. 18 beam excited field at the second bunch arrival.

The cavity field and energy excited as of the first bunch passage is expressed as

$$\Delta E_{1+} = qV_e = q\, f\, V_b$$
$$U_{1+} = \alpha V_b^2 \tag{5-1}$$

The voltage and energy of the cavity at the second bunch passage are

$$V_{b1+} = V_b\, e^{j\theta}$$
$$U_{2+} = \alpha (V_{b1+}\, e^{j\theta} + V_{b2+})^2 \tag{5-2}$$
$$= 2\alpha V_b^2 (1 + Cos\theta)$$

One the other hand, the energy loss of the second bunch is expressed as

$$\Delta E_{2+} = qV_e + qV_b\, Cos(\varepsilon + \theta) \tag{5-3}$$

Since energy loss of the two bunches equals to the stored energy as of the second bunch passage,

$$\Delta E_{1+} + \Delta E_{2+} = U_{2+} \quad . \tag{5-4}$$

Then the following equation is obtained,

$$2(q\,f - \alpha V_b) + (q\,Cos\varepsilon - 2\alpha V_b)Cos\theta - q\,Sin\varepsilon\,Cos\theta = 0 \quad . \tag{5-5}$$

This should be true for any θ, so that

$$\therefore \varepsilon = 0, \qquad V_b = \frac{q}{2\alpha}, \qquad f = \frac{1}{2} \tag{5-6}$$

These states that a bunch excites a cavity with the field in a decelerating direction when it passes a cavity, or in other words, it remains the decelerating field in the cavity. The passing particle itself feels the half of the excited field by the whole bunch

5.2 Long range wake field in a cavity

Long-range wake field excited in a cavity is expressed as[10]

$$W_L(s) = 2k_L\, e^{-\alpha\frac{s}{c}}\,(Cos(\bar{\omega}\frac{s}{c}) - \frac{\alpha}{\omega}Sin(\bar{\omega}\frac{s}{c})), \qquad \bar{\omega} = \sqrt{\omega_0^2 - \alpha^2}\ ,\ Q = \omega_0 / 2\alpha \tag{5-7}$$

where k_L is the loss parameter and α is the Q-value related parameter. In typical case with very high Q value, α=0 and the above equation becomes

$$W_L(s) = 2k_L\, e^{-\frac{\omega_L}{2Q}\frac{s}{c}}\, Cos(\omega_L\frac{s}{c}), \quad where\ k_L = \frac{\omega_L}{2}(\frac{R}{Q})_L \tag{5-8}$$

$$W_T(s) = 2k_T\, e^{-\frac{\omega_1}{2Q}\frac{s}{c}}\, Sin(\omega_1\frac{s}{c}) \tag{5-9}$$

The longitudinal wake field behaves cosine-like. The driving bunch is decelerated and it excites the field in the cavity. Even point-like bunch suffers from the wake field, deceleration, with losing kinetic energy. On the other hand, the transverse (dipole) wake behaves sine-like. It increases linearly in time at very short time, usually within the bunch. Point-like bunch does not suffer from the transverse wake field.

From here we evaluate the loss parameter or R/Q value of the cavity. For the longitudinal mode,

$$\left(\frac{R}{Q}\right)_L \equiv \frac{V^2}{2\omega U}\ [\Omega]\ ,\ V \equiv \int_0^L E_z(z)e^{jkz}\,dz, k = \frac{\omega}{c}, U = Stored\ energy \tag{5-10}$$

while for the transverse mode,

$$\left(\frac{R}{Q}\right)'_T \equiv \frac{(\partial V/\partial r)^2}{2\omega U}\frac{1}{k^2}[\Omega]\ ,\ \partial V/\partial r \equiv \int_0^L \frac{\partial E_z(z)}{\partial r} e^{jkz}\, dz\ , k=\frac{\omega}{c}, U = Stored\ energy \tag{5-11}$$

The longitudinal wake function is described as

$$W_L(s) \equiv -\frac{1}{Lq}\int_0^L E_z^{cmf}\, dz\ [V/C/m] = \sum_n 2k_{L,n}\, e^{-\frac{\omega_n}{2Q_n}\frac{s}{c}} Cos(\frac{\omega_n}{c}s) \tag{5-12}$$

For SW cavity case,

$$k_{L,SW} = \frac{V^2}{4U}/L = \frac{\omega}{2}(\frac{R}{Q})_L / L \quad , \tag{5-13}$$

while in TW cavity,

$$k_{L,TW} = \frac{E_0{}^2}{4u} \tag{5-14}$$

Here only the space harmonics of *n=0* contributes. When we consider the SW case, it is formed with superposition of two TW modes, propagating counter direction with each other, so that

$$E_z^{SW}(z,t) = E_0\{Cos\,\omega(t-\frac{z}{c}) + Cos\,\omega(t+\frac{z}{c})\} \quad . \tag{5-15}$$

The field calculated by SW mode is the case with t=0 in the above equation

$$E_z^{SW}(z,t) = 2E_0\, Cos\,\omega(\frac{z}{c}) \tag{5-16}$$

Therefore, E_0 can be evaluated as

$$E_0 = \frac{1}{L}\int_{-L/2}^{L/2} E_z^{SW}(z)\, Cos(\frac{\omega}{c}z) = \frac{V}{L} \quad . \tag{5-17}$$

When we consider the coupling of the beam to the TW mode, the relevant stored energy is only the forward wave, which is half of SW case.

$$k_{L,TW} = \frac{V_{SW}{}^2}{4(U_{SW}/2)}/L = \frac{V_{SW}{}^2}{2U_{SW}} \tag{5-18}$$

$$\therefore\ k_{L,TW} = \omega\left(\frac{R}{Q}\right)_L / L \tag{5-19}$$

Then the loss parameter of SW and that of TW are

$$k_{L,TW} = 2 \times k_{L,SW} \quad . \tag{5-20}$$

Let us evaluate from now the transverse loss parameter. Transverse field excited by a bunch with charge *q* passing a cavity with transverse position offset of *Δr*,

$$(\vec{E} + \vec{v} \times \vec{B})_T \tag{5-21}$$

so that the wake field due to this mode is

$$W_T(s) \equiv \frac{1}{L\, q\, \Delta r} \int_0^L (\vec{E} + \vec{v} \times \vec{B})_T^{cmf}\, dz \; [\frac{V}{C\, m^2}] = \sum_n \frac{2k_{T,n}}{\omega / c} e^{-\frac{\omega_n}{2Q_n}\frac{s}{c}}\, Sin(\frac{\omega_n}{c} s) \tag{5-22}$$

This can be expressed in SW and TW cases as follows. For SW case, we estimate using Panofsky Wenzel theorem that

$$(\vec{E} + \vec{v} \times \vec{B})_T^{cmf} = \frac{j}{\omega / c} \nabla_T E_z^{cmf} \tag{5-23}$$

If we apply this to eq. (4-62), the wake field becomes

$$W_T^0(s) \equiv \frac{1}{L\, q\, \Delta r} \frac{j}{\omega / c} \frac{\partial V}{\partial r} \quad . \tag{5-24}$$

The energy of the cavity excited by charge q with offset Δr is equal to the energy loss if the bunch interacting with the field excited by itself,

$$U(\Delta r) = \frac{1}{2} q \frac{\partial V}{\partial r} \Delta r = k_T^{SW} (q\, \Delta r)^2\, L \tag{5-25}$$

Where

$$k_T^{SW} = \frac{\omega}{2} k^2 (\frac{R}{Q})'_T / L \tag{5-26}$$

If we think the relation

$$W_T^0 = \frac{2k_T}{\omega / c} \tag{5-2}$$

The equation of (5-22) was found proven. This is for SW case. If we think the TW case as in the SW case,

$$k_{T,TW} = 2 \times k_{T,SW} \tag{5-28}$$

Therefore,

$$k_{T,TW} = \omega k^2 \left(\frac{R}{Q}\right)_T^{'} / L \tag{5-29}$$

And this relates between the loss parameter to the R/Q value in the transverse case.

5.3 Frequency scaling of R/Q value

Now we can estimate the frequency scaling of the parameters as follows;

	Per cavity	Per unit length
Longitudinal	$\left(\frac{R}{Q}\right)_L \equiv \frac{V^2}{2\omega U} \propto \frac{\lambda^2}{\omega\lambda^3} \propto 1$ $[\Omega]$	$\left(\frac{R}{Q}\right)_L / L \propto \omega$ $W_L \propto k_L \propto \omega\left(\frac{R}{Q}\right)_L / L \propto \omega^2$
Transverse	$\left(\frac{R}{Q}\right)_T^{'} \equiv \frac{(\partial V/\partial r)^2}{2\omega U}\frac{1}{k^2} \propto 1$ $[\Omega]$	$\left(\frac{R}{Q}\right)_T^{'} / L \propto \omega$ $k_T \propto \omega k^2 \left(\frac{R}{Q}\right)_T^{'} / L \propto \omega^4$ $W_T \propto \frac{k_T}{\omega} \propto \omega^3$

5.4 Calculation of R/Q of transverse mode in a pillbox cavity

Now, let us calculate the R/Q value of the transverse mode in a pillbox cavity. This is the most basic estimation for discussing the transverse dynamics. We calculate here the most typical dipole mode, TM1nl, in a pillbox cavity. The most typical and usually largest R/Q mode is TM_{110} mode. Taking the equation obtained in LINAC-I for pillbox modes,

$$\begin{aligned}
E_r &= -\frac{\beta_z}{K_c}\ Cos(\theta)\ J_1^{'}(K_c r)\ Sin(\beta_z z) \\
E_\theta &= \frac{\beta_z}{K_c^2}\ Sin(\theta)\ \frac{1}{r}J_1(K_c r)\ Sin(\beta_z z) \\
E_z &= \ Cos(\theta)\ J_1(K_c r)\ Cos(\beta_z z) \qquad where\, K_c = \rho_{1n}/a,\ \ \beta_z = l\pi/d \\
H_r &= -j\frac{\omega\varepsilon}{K_c^2}\ Sin(\theta)\ \frac{1}{r}J_1(K_c r)\ Cos(\beta_z z) \\
H_\theta &= -j\frac{\omega\varepsilon}{K_c}\ Cos(\theta)\ J_1^{'}(K_c r)\ Cos(\beta_z z) \\
H_z &= 0
\end{aligned} \tag{5-30}$$

The slope of E_z in r-direction on θ=0 plane at the beam axis becomes

$$\frac{\partial E_z(z)}{\partial r} = \frac{\partial}{\partial r} J_1(K_c r) = K_c [2 J_0(K_c r) - \frac{J_1(K_c r)}{K_c r}]\Big|_{r=0} = 1.5 K_c \tag{5-31}$$

And the value per cavity becomes

$$\begin{aligned} \partial V / \partial r &\equiv \int_{-L/2}^{L/2} \frac{\partial E_z(z)}{\partial r} e^{jkz}\, dz = 2\int_0^{L/2} 1.5 K_c\, Cos(kz)\, dz \; = 3K_c \int_0^{L/2} \; Cos(kz)\, dz \\ \therefore \partial V / \partial r &= \frac{3K_c}{k} Sin(\frac{kL}{2}) \end{aligned} \tag{5-32}$$

Then the R/Q per cavity becomes

$$\left(\frac{R}{Q}\right)_T' \equiv \frac{(\partial V / \partial r)^2}{2\omega U} \frac{1}{k^2} \; = \frac{2(\frac{3K_c}{k})^2 Sin^2(\frac{kd}{2})}{\omega \mu \pi d\, a^2 k^2 (\frac{\omega \varepsilon}{K_c})^2 J_1'^2(\rho_{1n})} \tag{5-33}$$

Hereafter, we note some comments on transverse (dipole) mode. Firstly note that TE mode cannot couple to beam because of no E_z field. Secondly, there are two polarizations in dipole modes with the same field pattern. The frequencies of these modes are almost the same, meaning these are almost degenerate. Therefore, it is necessary to separate in frequency for these modes to be stable unless the two polarizations can be divided by geometry condition.

6. Actual higher order mode examples

6.1 Superconducting nine-cell SW cavity

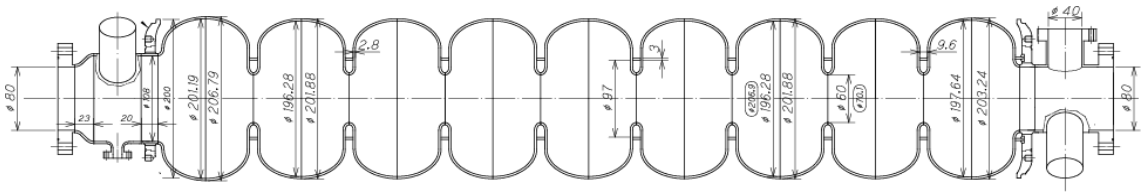

Fig. 19 Nine-cell SCC, superconducting cavity

In Fig. 19 is shown the cross section of the 9-cell superconducting cavity. Here we see that

1. Nine pillbox-like cells are connected by beam hole
2. Cells are almost identical, except for the end cells
3. Beam pipes at both ends are equipped with HOM extraction couplers

Higher order mode study on this cavity was performed. One of the results, the S21 parameters, the transmission from left end plate in beam pipe to the right, are shown in Fig. 20. Since this is 1.3GHz cavity for accelerating mode in TM010-like mode, the first HOM passband at 1.7GHz region is those of TE11-like mode. In this example, the red curve is the transmission excited from an antenna at the left end plane to the antenna at the same angle at the right end plate. In contrast, the blue line is the transmission between the antenna at 90 degrees apart between right end and left end. It is seen in the first two passband that the blue is lower than red, meaning these are dipole modes.

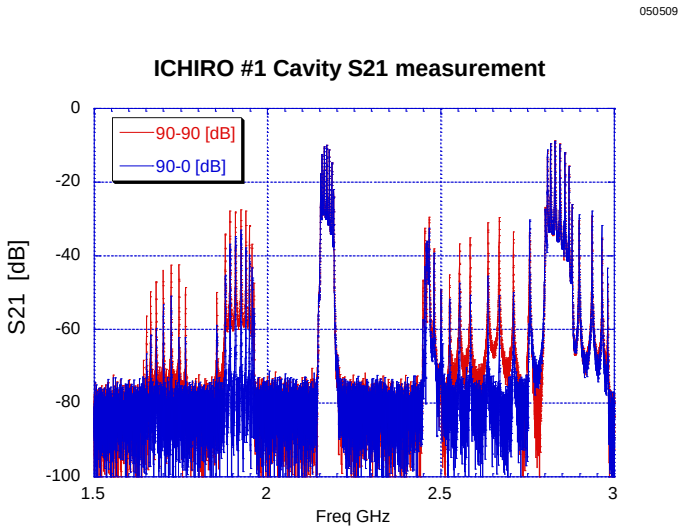

Fig. 20 S21 (transmission) spectra of SCC cavity.

In Fig. 21 are shown [Left] the schematic dispersion diagram up to very high frequency, [Center] the actual modal frequencies, and [Right] the nature of the coupling of the mode to the beam with showing those of the first passband. The diameter of the circle shows the degree of coupling. Those mode near to the phase velocity v_p near light velocity c couple more.

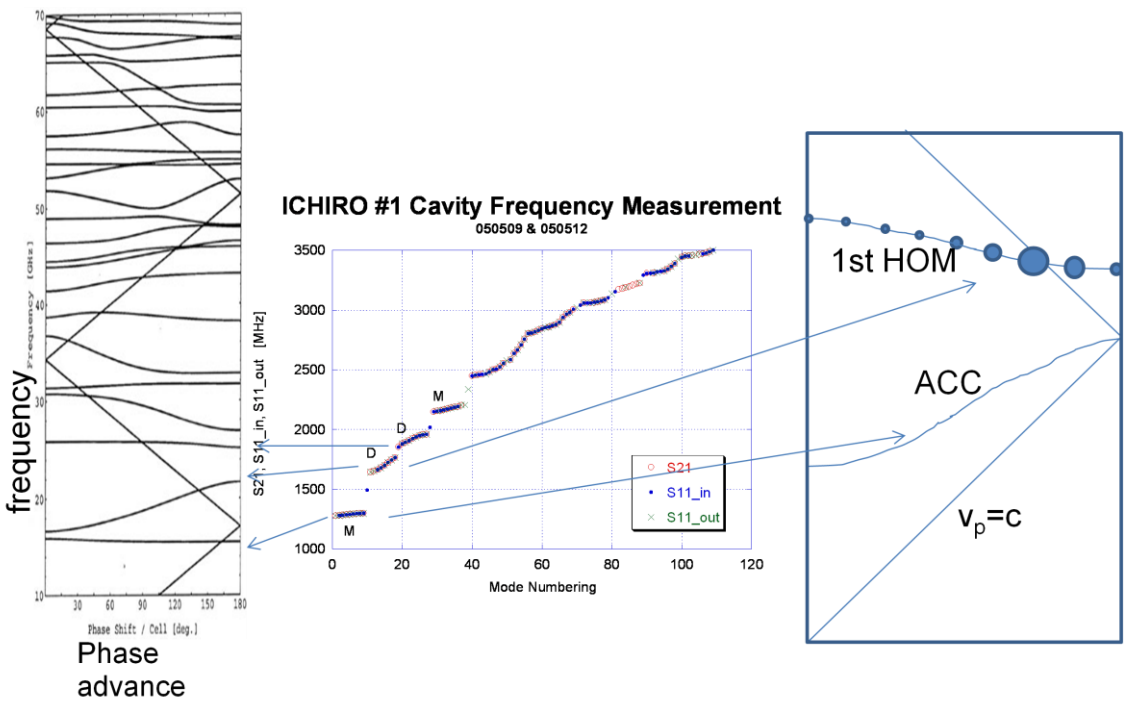

Fig. 21 9-cell SCC cavity: [Left] dispersion curves (schematic), [Center] actual mode frequencies, and [Right] the schematic excitation of the first passband with circles showing the coupling of the to the beam with the diameter in the figure.

6.2 Normal conducting TW detuned disk loaded structure

As an example of the normal conducting cavity, we show the case of X-band disk loaded structure (DLS) as shown in Fig. 22. Here, different from SCC case, the cell shape along the structure is continuously varying.

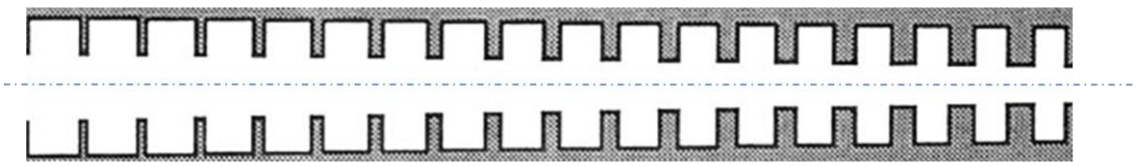

Fig. 22 Disk loaded structure with varying dimensional parameters.

The dipole mode frequencies are intentionally distributed as shown in [Right] of Fig. 23. This is realized by changing the cell parameters, (a,t), the beam hole aperture and disk thickness, along the structure as shown in [Left] of the figure. The relationship between (a,t) and dipole mode frequencies is shown in the contour plot in [Center] of the same figure. This design is called as "dtuned" as the dipole modes are varied to make the detuning effect against the coherent sum up of the dipole wake field.

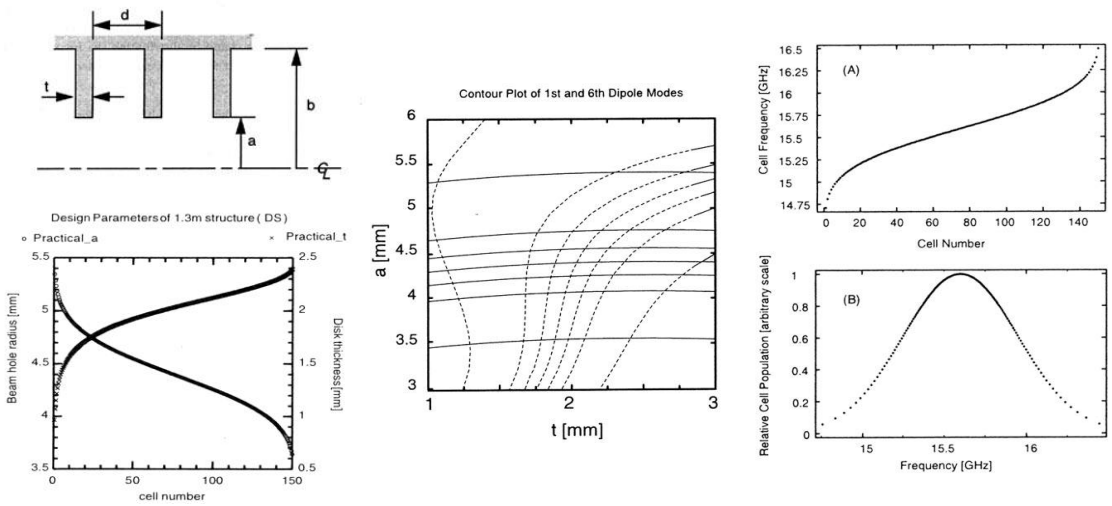

Fig. 23 [Right] Actual dipole mode frequency distribution along the structure and [Left] parameters to realize it. [Center] the dipole mode frequency contour plot versus geometry.

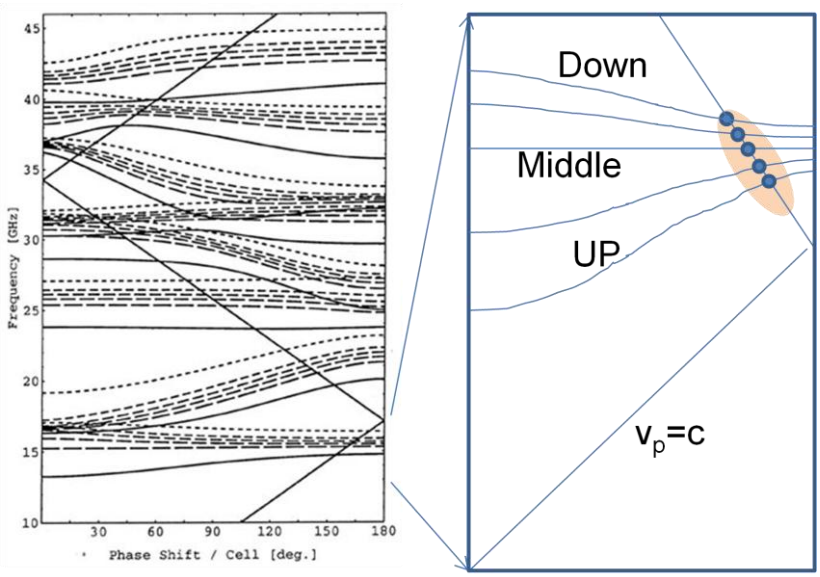

Fig. 24 Dispersion of detuned disk loaded structure.

In the Fig. 24 [Left], the dispersion curves are plotted up to very high frequency band. A batch of 6 passbands attributes to the same band but each representing the cells from upstream to downstream of the structure. By changing the design parameters along the structure, the dispersion curves thus vary. The coupling to the beam to the first passband is shown schematically in [Right] of the figure. The modes shown in dots near light velocity are mostly excited by beam. Fig. 25. This is the example of X-band 11.4GHz accelerating mode. The lowest three passbands are clearly seen, the lowest accelerator band, the second and the third the dipole modes.

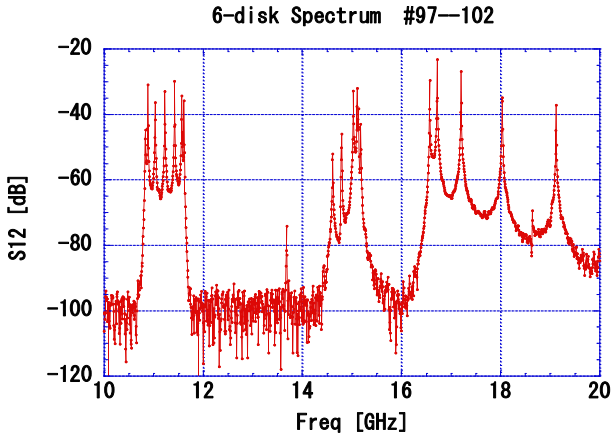

Fig. 25 Measured S21 spectrum for the cells near center of structure.

7. Ways of calculation of HOM

7.1 Various ways of treating structure geometry

There are many ways of calculating the multi-cell cavity or structure[11]. Firstly the equivalent circuit model[12] is most popular technique for analyzing coupled resonator system with many-cells. This assumes a finite number of modes in each cell and the coupling among adjacent cells and between modes.

Another way is to describe the disk loaded geometry with division at various relevant planes and connect between the adjacent areas with the field matching[13] in between. Typical cases are shown in Fig. 26.

The last way is those of numerical calculation in 2D or in 3D based on finite element method such as HFSS[14] or Ω2, Ω3[15] or finite different method such as MAFIA[16] and GdfidL[17].

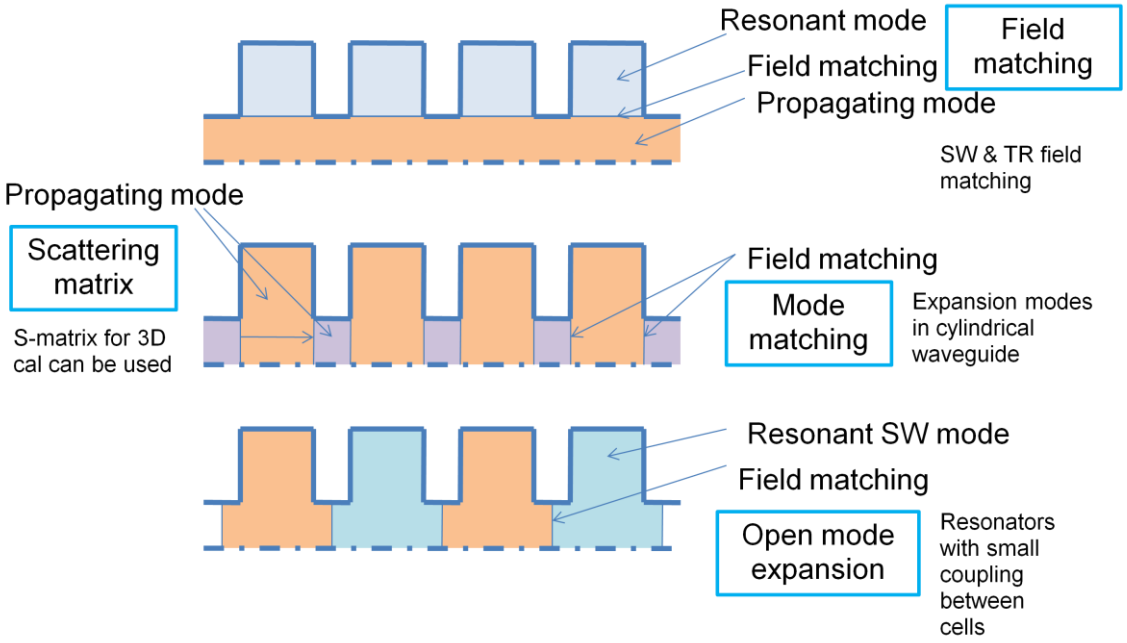

Fig. 26 Various mode matching techniques.

6.2 An detailed example: open mode expansion technique

Here we show an example of "open mode expansion" technique[18] in somewhat detail to discuss about the usual technique with using a finite number of modes to describe the whole system. This technique is based on the actual modes representing the modes sitting in each constituent cell in order to describe the whole coupled resonator system. The structure to be calculated is such as shown in Fig. 22. The dispersion curves of the transverse modes for any part of such a structure are shown as in Fig. 27.

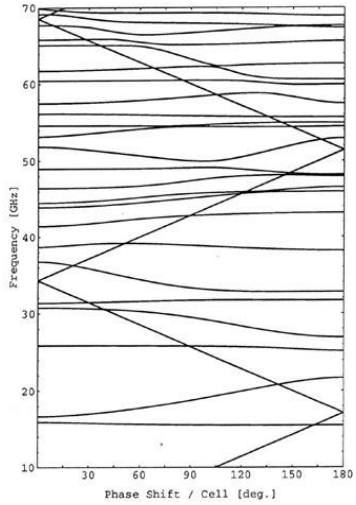

Fig. 27 Dispersion curves of typical DLS.

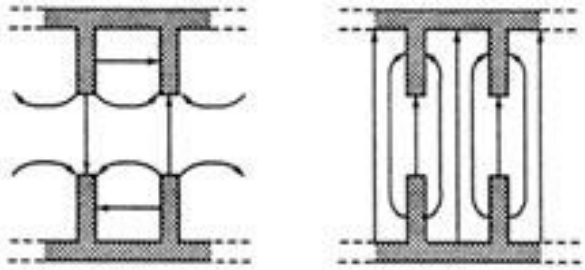

Fig. 28 Open mode field schematic.

In this model, the partition into cells is defined at the middle of the beam hole aperture, where the coupling between cells are happening. By doing so, the modes in each cell can be based on fairly physical modes, which can be understood physically well. There are various choices for the boundary condition at this partition plane. We took the "open" boundary condition, where the electric field is parallel to the partition as shown in Fig. 28. However, it is possible, for example, to take the "short" boundary condition. Both modes can be complete to describe the whole system mathematically. The actual open modes up to the eighth mode are shown in Fig. 29. These modes are calculated with numerical solver for several representing cells along the structure to get the parameters for the calculation.

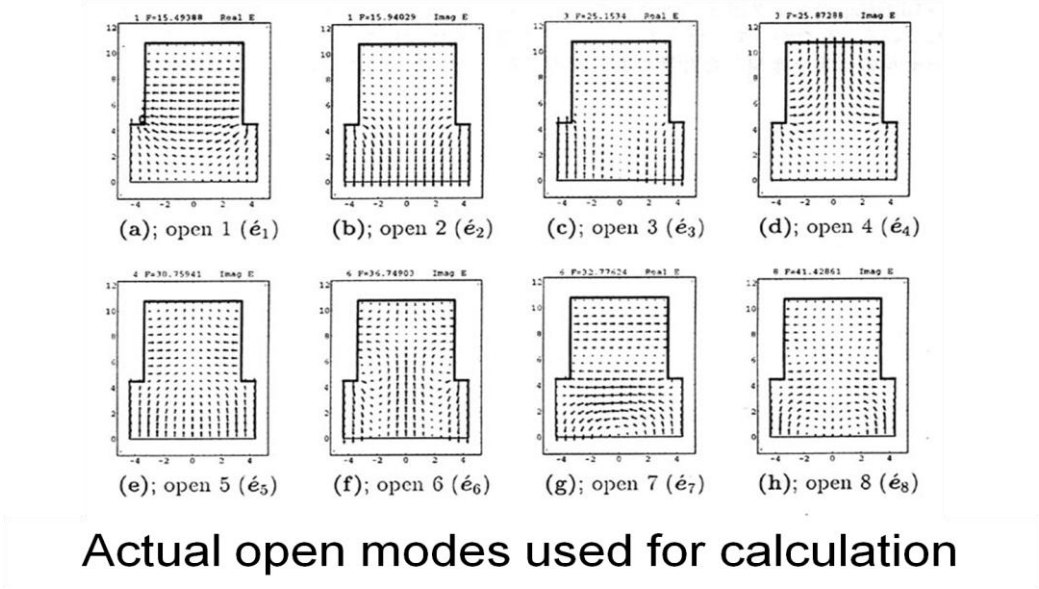

Fig. 29 Electric fields of actual open modes used for calculation.

Expanding with these open modes e_j

$$E(r,z)=\sum_{k=1}^{N_s}\sum_{n=1}^{8} a_j\, e_j^{open}$$

,

then the eigen value problem becomes

$$X\,a=\omega^2\,a$$

$$a\equiv(a_1,a_2,a_3,.....a_{8N})^T$$

where X represents the resonant behavior of the mode in each cell and the coupling between cells. This can be solved numerically to obtain the eigen solution of the whole structure. The result is shown such as shown in Fig. 30. Here each graph shows one of the modes with the field pattern decomposing into 8 open modes and the field at the location along the structure shown in the horizontal axis. The red numbers are the numbering of modes in frequency.

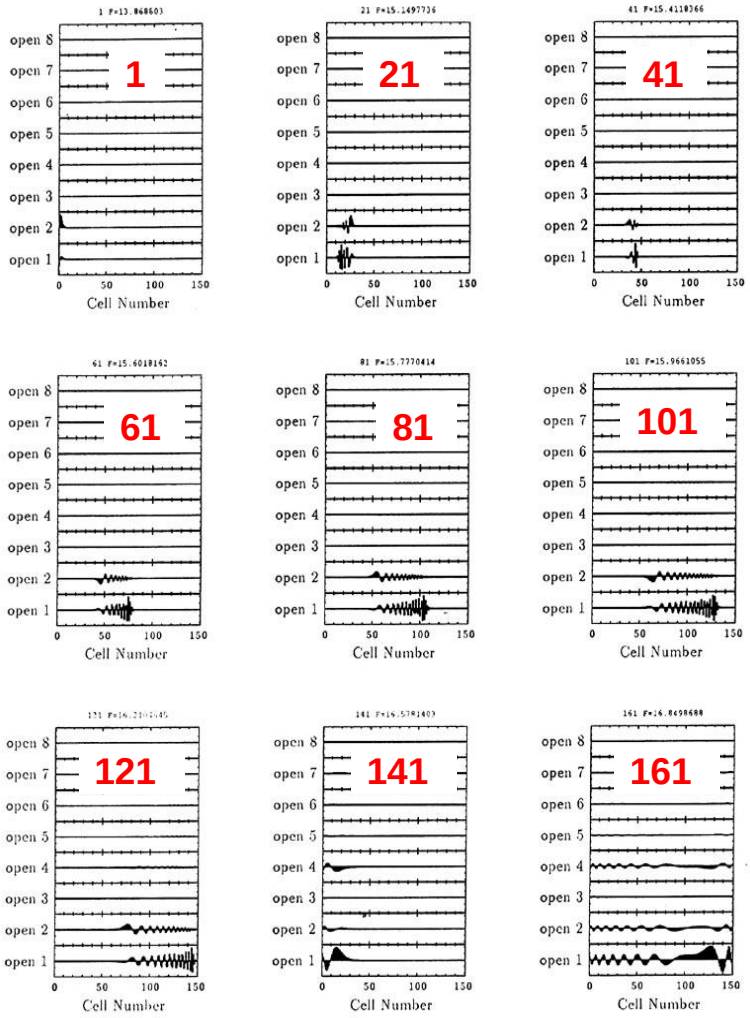

Fig. 30 Eigen vector of the model obtained.

From this result we can understand the physical nature of the system. In the lower frequency modes the fields are localized at the initial part of the structure while the location moves toward the downstream side as the modal frequency goes up. It is also shown that the lowest two open mode bases are the relevant field and they interact each other because they always appear at the similar location.

The kick factors are calculated from this result summing all the fields along the structure for all of the modes. The result is shown in Fig. 31. The resultant wake field is calculated by summing the contribution of all the modes based on these kick factors as shown in Fig. 32.

$$W_T(t) = \sum_{n=1}^{N} 2\,k_{T,n}\,Sin(\omega_n t)$$

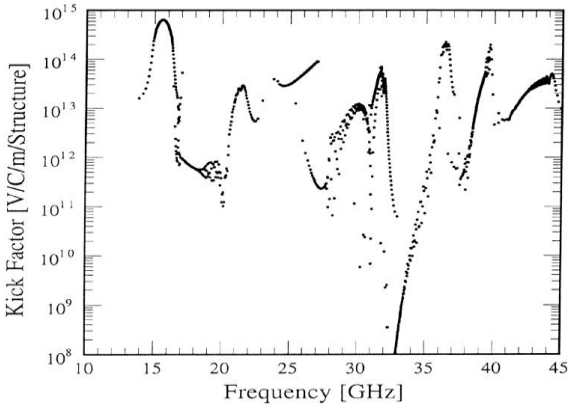

Fig. 31 Kick factors of all the modes.

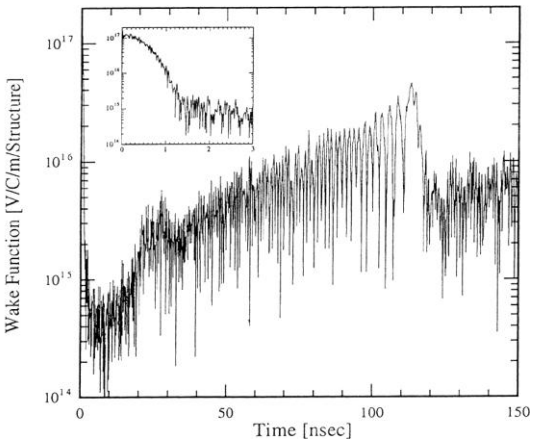

Fig. 32 Calculated wake field.

8. Cures against multi-bunch emittance growth by suppression of wakefield

8.1 Cures from structure design

There are two ways of suppressing the field. One is to align beam to modal axis which suppresses the excitation of dipole mode because no Ez field on axis. Another way is to suppress the excited wake field. In this chapter we discuss the latter issue. We also focus on transverse mode. The wake field of the transverse mode is expressed as

$$W_T(s) \propto \sum_n 2k_{T,n} e^{-\frac{\omega_n}{2Q_n}t} Sin(\omega_n t)$$

Here the damping term is expressed as

$$e^{-\frac{\omega t}{2Q_L}} \quad , \quad \text{where} \quad Q_L = \frac{\omega U}{P_{wall} + P_{ext}} \quad .$$

In usual accelerator cavities and structures, the intrinsic Q value, Q_{wall}, is very large. Therefore, it is not sufficient to suppress the excited wake field by wall loss of cavities.

$$\frac{\omega t_b}{2Q_L} \approx \frac{f\, t_b}{Q_L/\pi} \approx \frac{468}{10^{10}} \; for\; ILC, \; \approx \frac{6}{10^4} \; for\; CLIC << 1$$

In the ILC SCC cavity, the cavity is equipped with more than two HOM couplers. These HOM couplers damp the modes whose field touches to the couplers. This type of damping is established in the range of 10^5. This damping amount is not enough for damping at the next bunch but it contribute to the damping among the bunch trains, which is of the order of 10^3 bunches. For CLIC case, the aggressive damping is designed with opening big holes facing at each cell. This opening can reduce the Q value down to the order of 10. It means the wake field can be damped by the order of 10 at the following bunch.

Another way to effectively suppress the wake field at much shorter period at the following bunch needed for such as CLIC, is the introduction of the frequency spread of the excited modes,

$$W(t) \propto \int f(\omega) e^{j\omega t} d\omega$$

If the frequency spread $f(\omega)$ is large enough of the order of 10% of the frequency, the wake field which is the Fourier transform of the kick factor is naturally damp as inversely proportional to the frequency spread, resulting in the damping in the order of 10 RF cycles. The basic nature is shown in the Fig. 33 in the view point of the cancellation among the modes. Here we assume the kick factor

for each mode the same. Actually the density of the kick factor should be distributed well to make the wake field characteristics in a better shape in longer period.

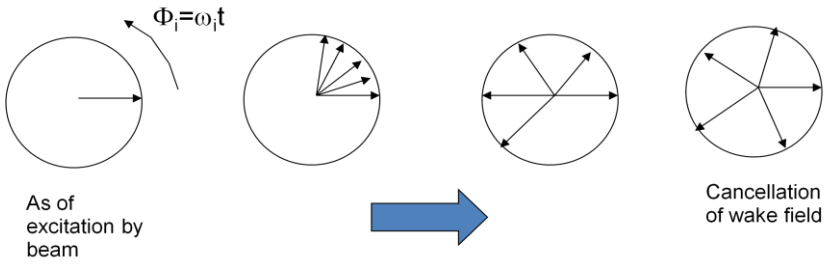

Fig. 33 Cancellation of fields in excited modes.

In a sophisticated design of a detuned structure, the distribution of kick factor times the density of the mode is designed to be Gaussian[19]. This makes the wake field damping exactly as Gaussian like. An example is shown in Fig. 35 for GLC/NLC structure[20]. In this design, it should be noted that the wak damping of the order of Q~1000 is implemented by the coupling of the excited modes in the accelerator cell to the damping manifold running parallel to the structure. This is shown as the top transmission line shown in Fig. 34. The actual shapes of the cell with such manifold are shown in Fig. 36. The coupling between cell modes and manifold modes is realized by a thin channel which makes the effective Q value of the cell to be ~1000. In the dispersion diagram, the coupling appears as the avoided crossing of the dispersion curves which appears where any physical interaction exists.

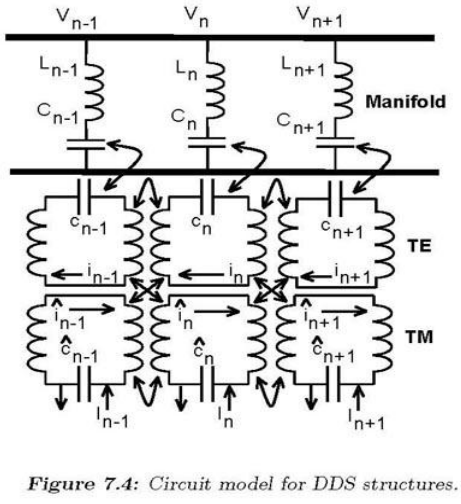

Figure 7.4: Circuit model for DDS structures.

Fig. 34 Equivalent circuit modeling of damped detuned structure.

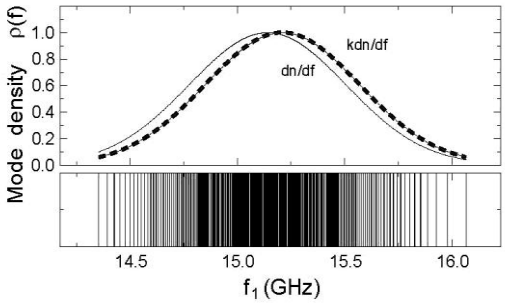

Fig. 35 Gaussian distribution of k dn/df.

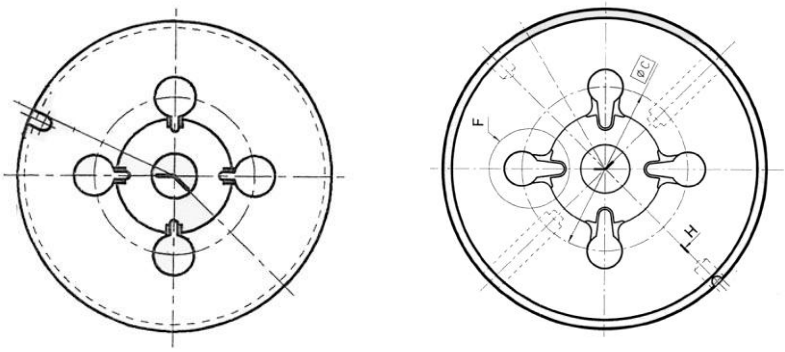

Fig. 36 Actual cell shape with four manifolds running parallel to the beam axis.

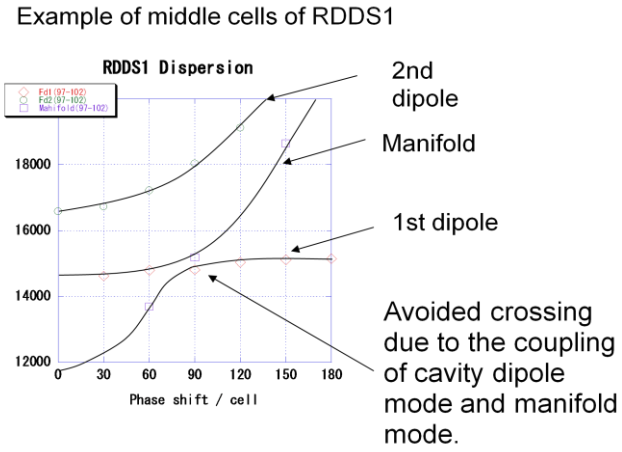

Fig. 37 Dispersion diagram showing the avoided crossing which represents the coupling between the lowest mode and manifold mode.

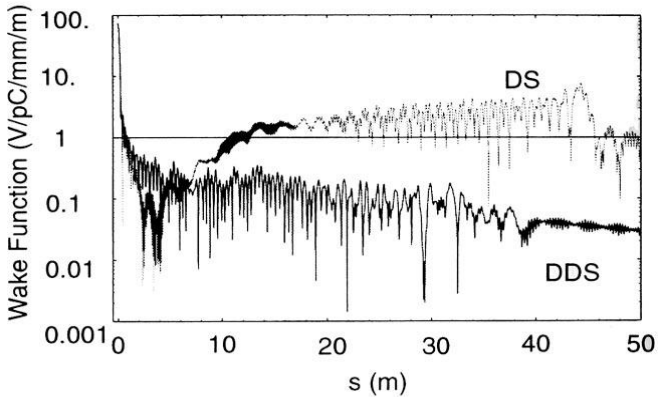

Fig. 38 Calculated wake field for two cases. DS: detuned structure and DDS: damped detuned structure.

In Fig. 38 are shown the wake fields for two cases; DS detuned structure and DDS damped detuned structure. In DS case, the rising of the wake appears at s=10m, which is due to the finite spread of the frequency distribution. The final big rise at s~45m is due to the re-coherence of the mode due to the finite number of modes available which make the mode-to-mode frequency spacing finite. The difficulties mentioned here for DS can be solved by introducing medium damping in DDS scheme. The figure clearly shows the damping nature by moderate Q value.

The wake field can be measured by such as ASSET[21] of SLAC. The transverse kick received by the witness electron bunch was measured by changing the offset of the preceding driving positron bunch. The results are shown in Figs. 39 and 40. The case of Fig. 40 shows the comparison of the measured and calculated with practical frequency errors. From these examples, we can conclude that the detuning method can practically be applied in a controlled manner.

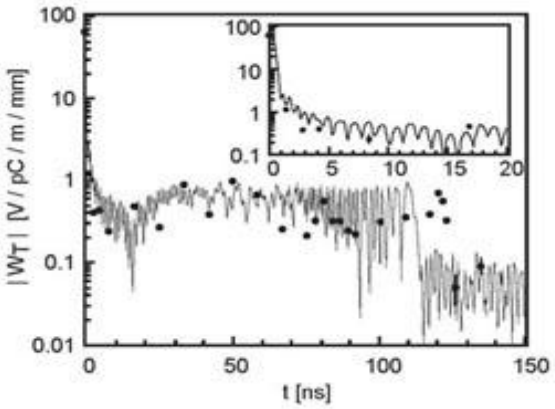

Fig. 39 Calculated wake field of DDS and measured data point shown in solid circles.

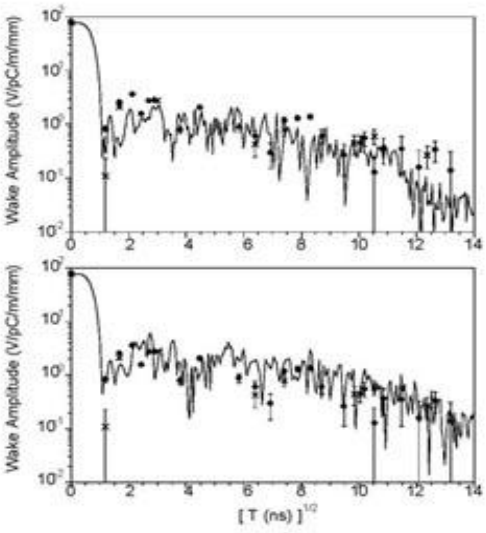

Fig. 40 Calculated wake field of DDS with a frequency error of 5MHz (top) and 12MHz (bottom).

8.2 The DDS structure in practice

The DDS structure is a series of regular cells with the detuning profile on their cell parameters along the structure. In Fig. 41 is shown a typical design example. Manifold is running along the structure and it ends with extraction port to outside. The most basic and essential characteristics to realize the detuning is to carefully control the dipole mode frequencies. In the example of Fig. 42, the frequency of the accelerating mode is controlled by varying the cell radius as the production of

cells along the structure. In this process, the frequency of the accelerating mode is within 1MHz so that the dipole mode frequency error is 1.5 times this value. This means that the frequency control of the dipole mode will be within 2MHz, which is usually well below the tolerance of the dipole mode.

In Fig. 43 shows the measurement of the first dipole, the second dipole and the manifold mode along the structure. Eight curves for each passband show those of the cells near input coupler, the middle and the last part of the structure. The measurement confirmed the frequency error information of the structure. In this structure, the wake field was measured and shown in Fig. 44 where the calculation is also plotted. The good frequency control made the wake field well meeting the design value.

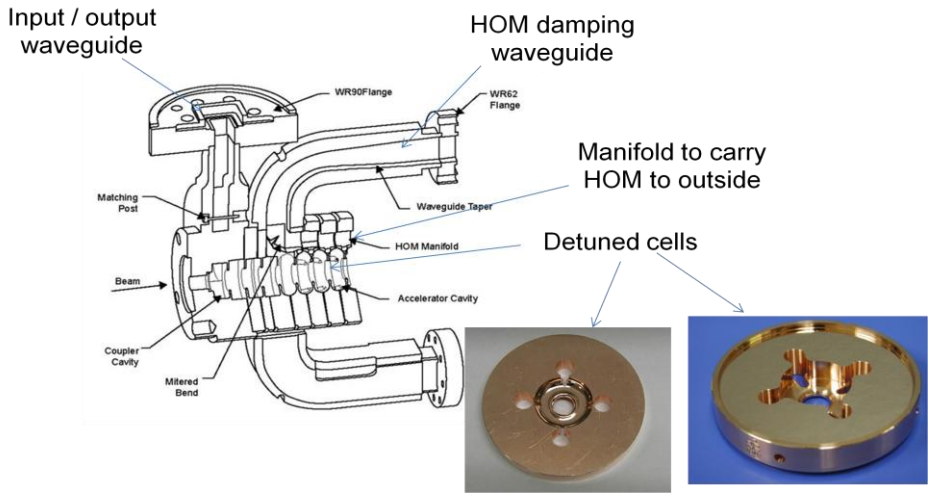

Fig. 41 The practical design of DDS structure and photos of DDS cells.

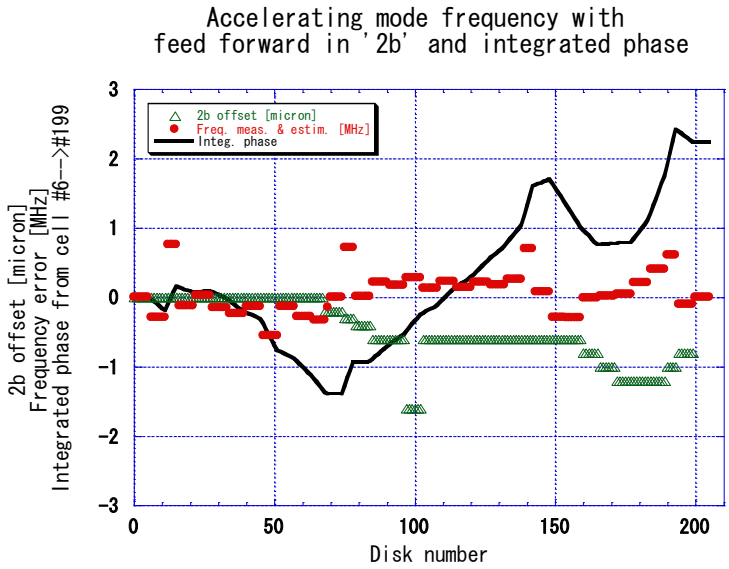

Fig. 42 Example of the precise frequency control of dipole modes.

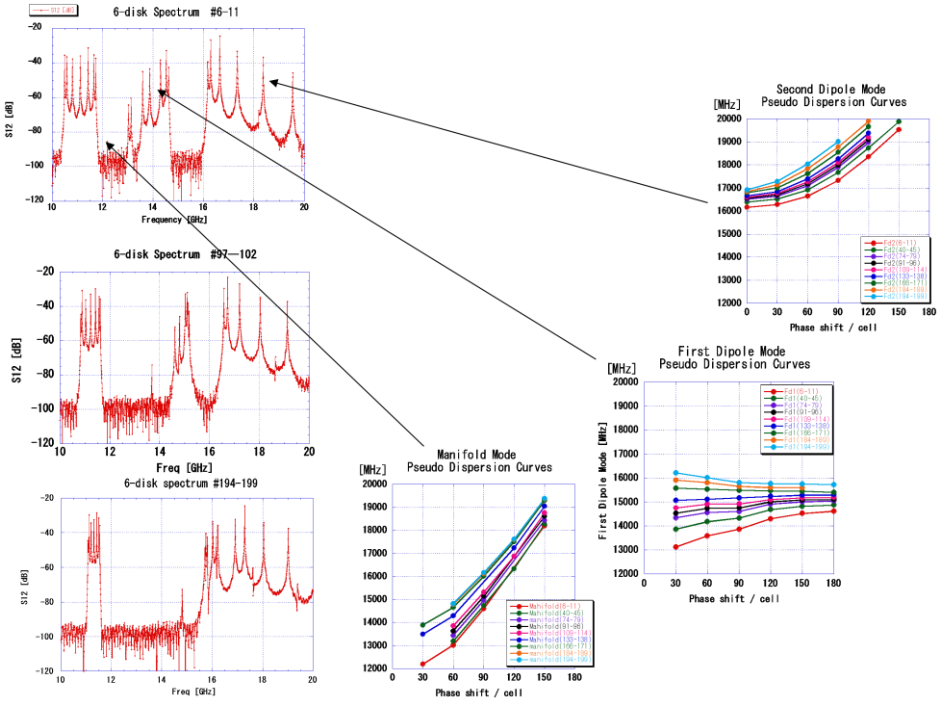

Fig. 43 Measured spectra of transmission measurement for 6 cells of some part of the acceleration structure.

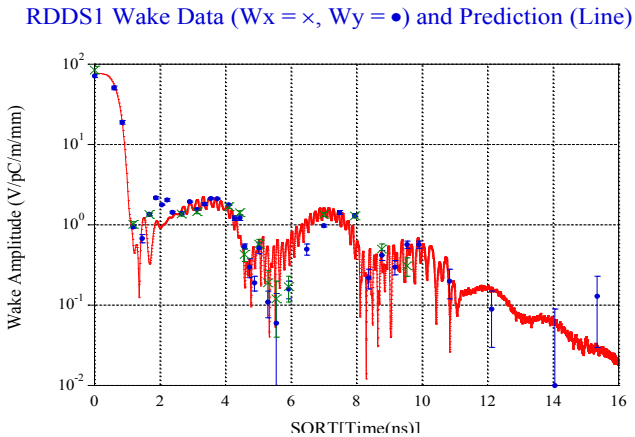

Fig. 44 calculated wake field and measured one for RDDS structure where the frequencies of the dipole modes are carefully controlled within a few MHz level.

9. Alignment of linac

In this chapter, various methods to align the accelerator structure are described.

9.1 One-to-one alignment

If every BPM is aligned perfectly to the magnetic center of each quadrupole magnet, it is easy to adjust the beam with respect to those magnets by just aligning the beam with zeroing the BPM reading.

Changing the Q strength makes the change in the transverse kick and this change can be measured at the downstream BPM's to know the beam position w.r.t. the Q center where the BPM is assumed to be perfectly aligned.

It is therefore the most straightforward way but suffers from errors in BPM reading and BPM misalignment w.r.t. Q magnet, etc.

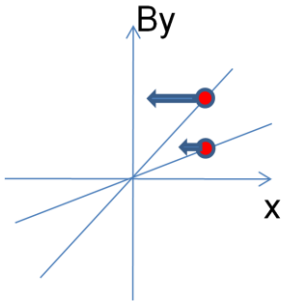

Fig. 45 Zeroing the BPM reading.

There were invented better ways of correcting the beam positions more globally, such as DF or WF correction schemes described below.

9.2 Dispersion free steering

The equation of motion in the transverse plane is expressed similar as in (4-3)

$$\frac{1}{\gamma(s)}\frac{d}{ds}\gamma(s)\frac{d}{ds}x(s;z,\delta)+(1-\delta)K[x(s;z,\delta)-x_q] = (1-\delta)G+\frac{1-\delta}{\gamma_0(s)}N r_e\int_z^{\infty}dz'\int_{-\infty}^{\infty}d\delta'\,\rho(z',\delta')W_{\perp}(s;z-z')[x(s;z',\delta')-x_a] \quad , \quad (9\text{-}1)$$

with

$$K(s)=\frac{e}{p_0 c}\frac{dB_y}{dx},\quad G(s)=\frac{e}{p_0 c}B_y \quad . \quad (9\text{-}2)$$

Here the first term in left hand side is the acceleration in the transverse plane, the second term the focusing term from the linac optics with the variation of focusing effect depending on the energy variation δ and the position measured w.r.t. he Q magnet center x_q. The first term in the right hand side is the kick by steering elements and the second term from wake field effect. The wake field is given as the offset from the structure alignment x_a.

Let us assume the beam to be consisted of two parts as shown in Fig. 46. The left figure represents the uncorrelated energy spread, meaning that the energy spread exists even at the same position of the bunch. This situation can be written in the difference orbit of the second part with respect to the first part as

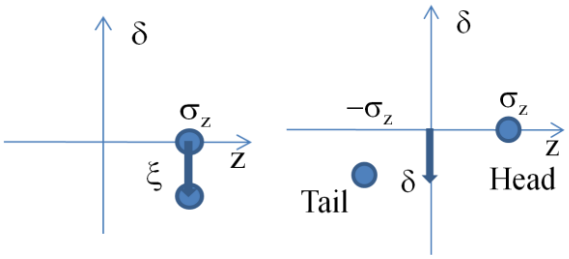

Fig. 46 [Left] correlated energy spread and [Right] uncorrelated energy spread.

$$\Delta x_d = x(\sigma_z, 0) - x(\sigma_z, \xi) \quad . \tag{9-3}$$

On the other hand, the correlated energy spread is shown in the right figure case. Here the difference orbit is written as

$$\Delta x_w = x(\sigma_z, 0) - x(-\sigma_z, \delta) \quad . \tag{9-4}$$

This case represents the bunch energy varies along the position z within the bunch.

In case of no wake field, the equation (9-2) can be written as

$$\begin{aligned} &\frac{1}{\gamma(s)}\frac{d}{ds}\gamma(s)\frac{d}{ds}\Delta x_d(s;\sigma_z,\xi) + K(s)\Delta x_d(s;\sigma_z,\xi) \\ &\quad = \xi(G(s) \;+\; K(s)[\, x_q(s) - x(s;\sigma_z,0)\,] \end{aligned} \quad . \tag{9-5}$$

Each term in the right hand side represents 1. the steering and 2. the orbit offset at the Q magnet.
If the wake field ON, it is expressed as

$$\begin{aligned} &\frac{1}{\gamma(s)}\frac{d}{ds}\gamma(s)\frac{d}{ds}\Delta x_w(s;\sigma_z,\delta) + K(s)\Delta x_w(s;\sigma_z,\delta) \\ &\quad = \delta\, G(s) \;+\; \delta K(s)\,\{x_q(s) \;- x(s;\sigma_z,0)\} \\ &\qquad -\frac{N r_e}{2\gamma_0(s)}\, W_\perp(s,2\sigma_z)\,\{(x(s;\sigma_z,0) - x_a(s)\} \end{aligned} \tag{9-6}$$

The first two terms in the right hand side represents the same as in (9-5) while the last term represents 3. the wake field effect. These two equations are the basic for the DF and DW steering scheme.

In the first order approximation, the solutions for these are written as the transferred position originated from the kick at *s'* upstream. Without wake field,

$$\Delta x_d(s;\sigma_z,\xi) = \int_0^s ds' R_{12}(s,s')\xi\{G(s') + K(s')[x_q(s') - x(s';\sigma_z,0)]\} \tag{9-7}$$

The minimization of Δx_d is equivalent to locally minimize the following value,

$$\begin{aligned} & G(s') + K(s')[x_q(s') - x(s';\sigma_z,0)] \\ & = [G(s') + K(s')\, x_q(s')] - K(s')\, x(s';\sigma_z,0)] \end{aligned} \quad , \tag{9-8}$$

where the right hand side expresses the cancellation of the effect due to the Q-magnet misalignment by local correction. In practice, from the i'th BPM reading m_i and its difference Δm_i with their predicted values, x_i and Δx_i minimization does dispersion free correction trying to minimize the following value,

$$\min\left(\sum_{i=1}^{N_{BPM}} \frac{x_i^{\,2}}{\sigma_{prec}^2 + \sigma_{BPM}^2} + \frac{\Delta x_i^{\,2}}{\sigma_{prec}^2}\right) \quad , \tag{9-9}$$

where σ_{prec} and σ_{BPM} are the precision of the BPM reading and the resolution of the BPM reading.

9.3 Wakefield free steering

Similar approach is applied for the case with the wake field. In the first order approximation, the solutions for these are written as the transferred position originated from the kick at s' upstream

$$\begin{aligned} \Delta x_w(s;\sigma_z,\delta) = \int_0^s ds' R_{12}(s,s')\delta\,[G(s') + K(s')\{x_q(s') - x(s';\sigma_z,0)\,] \\ - \frac{N r_e}{2\gamma_0(s')} W_\perp(s',2\sigma_z)\,\{x(s';\sigma_z,0) - x_a(s')\} \end{aligned} \tag{9-10}$$

The minimization of Δx_w is equivalent to locally minimize the following value,

$$\begin{aligned} & \delta[G(s') + K(s')\{x_q(s') - x(s';\sigma_z,0)\,] - \frac{N r_e}{2\gamma_0(s')} W_\perp(s',2\sigma_z)\,\{x(s';\sigma_z,0) - x_a(s')\} \\ & = \delta[G(s') + K(s')\, x_q(s')] - \{\delta K(s') - \frac{N r_e}{2\gamma_0(s')} W_\perp(s',2\sigma_z)\}\, x(s';\sigma_z,0) + \frac{N r_e}{2\gamma_0(s')} W_\perp(s',2\sigma_z)\, x_a(s') \end{aligned} \tag{9-11}$$

where the three terms in the right hand side are those from 1: misalignment of the Q-magnet, 2: wake field correction, and 3: structure misalignment. Wake field term cannot be cancelled out by δ term because of constant W_t while alternating nature in K(s'). However, if we take only QF or only QD, then the correction of W_t can be realized. In practice, from the i'th BPM reading m_i and its

difference Δm_i with their predicted values, x_i and Δx_i, the minimization does wake field free correction;

$$\min\left(\sum_{i=1}^{N_{BPM}} \frac{x_i^{\,2}}{\sigma_{prec}^2+\sigma_{BPM}^2}+\frac{\Delta x_i^{QF\,2}}{2\sigma_{prec}^2}+\frac{\Delta x_i^{QD\,2}}{2\sigma_{prec}^2}\right) \quad , \tag{9-12}$$

where the Δx_i^{QF} and Δx_i^{QD} are those difference orbit due to the variation of only QF or QD. The correction example is shown in the reference[22]. The result is shown in the table below.

Method	ε_y	Trajectory rms
1-to-1	$23\,\varepsilon_{y0}$	72 μm
DF	$9\,\varepsilon_{y0}$	55 μm
WF	$1\,\varepsilon_{y0}$	44 μm

9.4 Alignment with using excited field in the accelerator structure

If we measure dipole mode in a structure, we can estimate the position of beam which excites the mode. The coupling of the mode to the beam transverse position is linear. If the modal frequency depends on the position of the mode, as discussed in section 6-2 or 8-2, it can distinguish the beam position by filtering the excited field in frequency.

In such a cavity as ILC, it can be done with using the power from HOM couplers. In such cavity as CLIC, it can be done with extracted power from manifold or damping waveguide. Both directions x and y are measured with distinguishing two modes in different polarizations, almost degenerate but with some frequency difference unless distinguished by other means.

In Fig. 47 are shown the power and the phase of the excited field. As shown in the figure, the power is quadratically vary as the beam transverse offset, which is consistent to the linear coupling of the beam to the transverse mode. The phase changes the sign when the beam crosses across the axis and this behavior can be utilized to know which direction the beam is offset. The actual position of the beam with respect to the modal center was measured in one of the DDS structure. The result is shown in Fig. 48. It was found that the structure bending was confirmed with beam in the order of a few micron level. The method will be the very basic alignment tool for the linear collider application

which needs tight alignment tolerance. Especially the ILC case with the SCC cavities located in the vessel

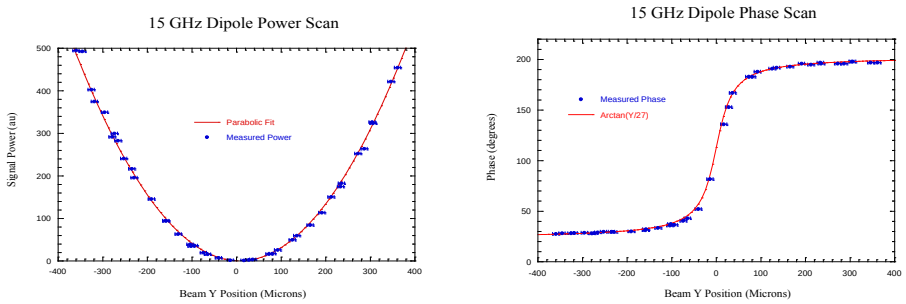

Fig. 47 [Left] Power excited by beam and [Right] Phase of the excited field.

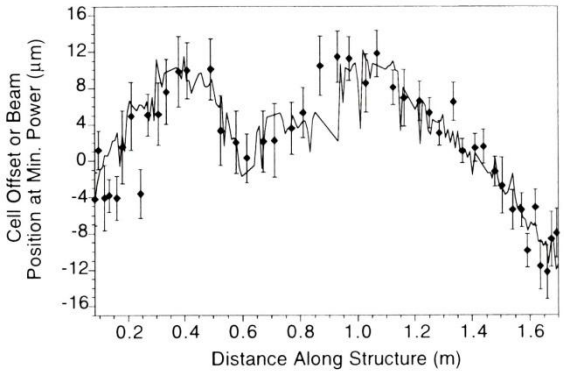

Fig. 48 Accelerator bending [dots] measured by beam and [line] by coordinate measurement machine.

10. More for LC not mentioned yet

10.1 Dark current issue

Dark current is a stable emission of electrons under high field. The DC field emission leading to the dark current is the tunneling feature of electron migration near surface. It is studied by Fowler-Northeim[23] and the current is expressed as below.

$$i_{FE,\,DC} = F\,E_0^2\,Exp(-\frac{G}{E_0}) \quad [A m^{-2}], \qquad F = 1.54\times10^{-6}\times10^{4.52\phi^{-0.5}}\,\phi^{-1},\; G = 6.53\times10^{9}\,\phi^{1.5} \tag{10-1}$$

Here work function and field enhancement factor play important roles. Actually the field E_0 is replaced by the local field βE_0. The ϕ is the work function of the surface. This DC current form can be extended to the alternating RF field as derived by J. Wang and G. Loew[24] as

$$i_{FE,\,RF} = F\,E_0^{2.5}\,Exp(-\frac{G}{E_0}) \quad [A m^{-2}], \qquad F = 5.7\times10^{-12}\times10^{4.52\phi^{-0.5}}\,\phi^{-1.75},\; G = 6.53\times10^{9}\,\phi^{1.5} \tag{10-2}$$

This dark current exists in an RF field, whether or not in SW and TW or in NCC and SCC.

If such dark current exists, the electrons will be accelerated by the accelerating field and hit the cavity surface and deposit energy locally. It may lead to the quenching of superconducting material or the collision with material may produce secondary electrons to be mass-produced iteratively. Such accelerated current will hit other places and may cause the misreading of the downstream BPM. Most of the electrons thus extracted are usually defocused by the strong Q magnetic field so that it cannot travel for a long distance. However, the electrons can be trapped in the RF field and can be accelerated to a fairly high energy before reaching to such defocusing devices.

There are many numerical simulations of the dark current in the structure. However, a simple analytical estimate gives the basic characteristics of the capture mechanism in the linac[25]. Below we describe such mechanism and derive the minimum threshold field for such capture mechanism. The acceleration field is expressed as the summation of all space harmonics in the periodic structure as below.

$$E_z = \exp j(\omega t - k_z z)\sum_{n=-\infty}^{n=\infty} -j\,E_n\,J_0(k_{rn} r)\exp^{-2j\pi n z/d}$$
$$k_{rn} = k^2 - (k_z + 2\pi n/d)^2 \tag{10-3}$$
$$k = \omega/c = 2\pi/\lambda$$

$$\frac{d\gamma}{dz} = -\sum_{n=-\infty}^{n=\infty} \varepsilon_n J_0(k_{rn}) Sin(\theta + \frac{2\pi n z}{d})$$
$$\varepsilon_n = e E_n / m_0 c^2 \ , \quad \theta = \int (\frac{1}{\beta_p} - \frac{1}{\beta}) dz \tag{10-4}$$

The acceleration can be performed along a finite distance with the phase slip θ. If, $\beta_p \sim \beta$, then θ is slowly varying function. Therefore, only n=0 becomes dominant for acceleration.

$$\frac{d\gamma}{dz} = -\varepsilon_0 Sin(\theta) \quad and \quad \frac{d\theta}{dz} = \frac{k}{\varepsilon_0}(\frac{\sqrt{p^2+1}}{\beta_p} - p) + A \tag{10-5}$$

Finally, by combining (10-4) and (10-5),

$$Cos(\theta) = \frac{k}{\varepsilon_0}(\frac{\sqrt{p^2+1}}{\beta_p} - p) + A \quad . \tag{10-6}$$

The plot of the contour of this equation is shown in Fig. 49. Here the momentum *p* relates to the energy of electrons as

$$\frac{p}{m_0 c} \equiv \sqrt{\gamma^2 - 1}$$

In the structure with slow phase velocity such as β_p=0.5, the electrons oscillate as shown in the left figure. If β_p=1 then A=Cos(θ_m) when approaching at *p* infinity and the phase freezes and the electrons are accelerated to very high energy without phase slip any more, as shown in the red arrows.

$$Cos(\theta) - Cos(\theta_m) = \frac{k}{\varepsilon_0}(\sqrt{p^2+1} - p) \tag{10-7}$$

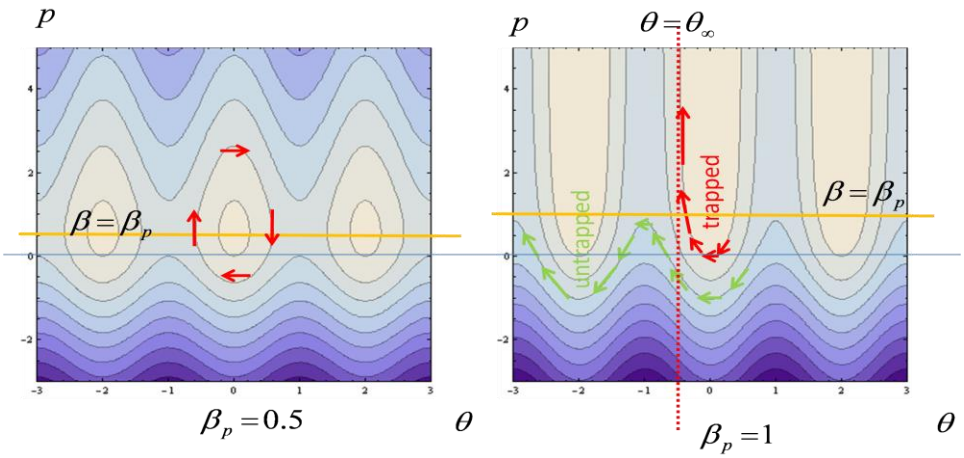

Fig. 49 Momentum versus phase of electrons in linac.

The minimum field ε_0 for being tramped, equivalent to being maximum in left-hand side,

$$Cos(\theta) - Cos(\theta_m) = 2$$

For zero-energy electron, p=0, to be captured, the minimum field becomes

$$E_{acc}^{threshold} = \frac{\pi m_0 c^2}{e\lambda} \tag{10-8}$$

which results in E_{acc}=7 MV/m at 1.3GHz for ILC and E_{acc}=61 MV/m at 11.424GHz for CLIC. It its to be noted that in both cases the design accelerator gradients are higher than this trap threshold.

10.2 Tolerable trip rate

Before closing this lecture, we discuss one of the important requirements for obtaining the high integrated luminosity. For this purpose, it is important to keep the instantaneous luminosity high. Once some failure happens in some cavity, the power feeding the cavity or the bunch of cavities is shut off. Then, the power or pulse width will be recovered taking some number of pulses starting from a little lower power level. During this period, the cavities in recovering mode are off in timing from acceleration for the linac if being powered by independent power supply. In such a system as CLIC two beam scheme, the off-timing operation cannot be applied and gradual power recovery is needed. During this recovery period, other cavities than nominal should be used to keep the beam energy. Therefore, linac needs extra acceleration capability than the nominal one. These extra spare cavities or the extra power/gradient capability is required.

Let us assume the compensation with spare cavities shown with red line in the figure below.

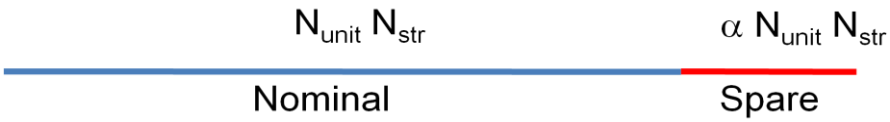

The number of failures during the recovery time for a cavity is expressed as

$$N_{unit} N_{str} R_{fail} T_{rec} \quad , \tag{10-9}$$

where R_{fail} is the failure rate for a cavity, 1 trip per N pulses, T_{rec} the recovery time in the unit of pulses, N_{str} and N_{unit} the number of unit per linac. This number should be less than the number of spare units.

$$N_{unit} N_{str} R_{fail} T_{rec} < \alpha N_{unit} \tag{10-10}$$

Then the tolerable failure rate is

$$R_{fail} < \frac{\alpha}{T_{recov} N_{str}} \quad . \tag{10-11}$$

Let us assume an example below.

$$N_{unit} = 3000$$
$$N_{str} = 8$$
$$T_{rec} = 60\,s \times 50\,Hz$$
$$\alpha = 0.01$$

In this case,

$$R_{fail} < 4 \times 10^{-7} \tag{1-12}$$

so that we understand that the tolerable rate is of the order of 1 trip / million pulses or less.

The failure rate should be decreased or the accelerating gradient margin should be increases to stably keep the luminosity. For the ILC SCC cavity, it is needed to increase the quench field level by improving cavity itself, to suppress the field emission dark current by surface improvement, to increase Q_0 and to make the life of the tuning system long. In the NCC cavity, it is essential to reduce the breakdown rate. The trigger mechanism of the breakdown is not well understood yet, but possible source of trigger to breakdown should be minimized. Some of them are such as the surface chemical quality, dusts on surface, micro protrusions and the temperature rise within a pulse called as pulse heating. The last is not least important. The pulse heating is the surface energy deposit within pulse duration, which diffuses as the heat diffusion in the material body. This phenomenon is shown in the figure below.

The surface temperature rise is written[26] as

$$\Delta T = \frac{1}{2} R_s \left| H_s \right|^2 \frac{2\sqrt{T_p}}{\rho c_\varepsilon \sqrt{\pi \alpha_d}} \tag{10-13}$$

where H_s is the surface magnetic field, T_p the pulse width, α_d the diffusion constant, ρ density of material, c_ε specific heat. In copper case, ΔT becomes as high as 270degC.

The surface heating at the very surface make the stress too large and the crystal boundary may suffer from the cracking and so on such as shown in Fig. 50[27]. It can be speculated that such cracks may result in the trigger source of

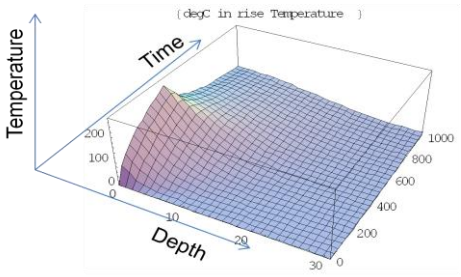

Fig. 50 Pulse surface heating.

breakdowns. Therefoe, such high surface temperature should be suppressed.

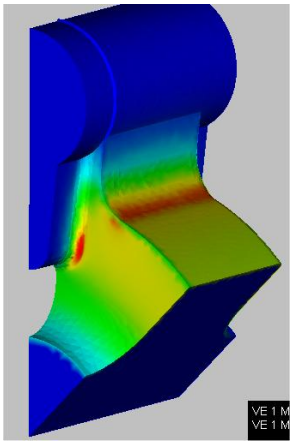

Fig. 51 Surface magnetic field.

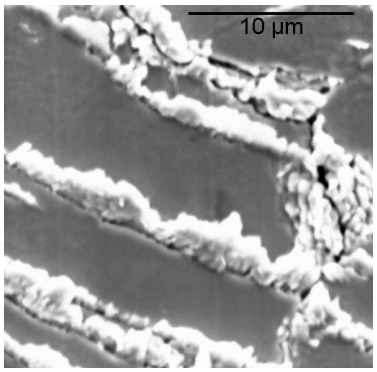

Fig. 52 Cracking on copper surface.

In Fig. 51 is shown the magnetic field distribution around the DDS cells. There are multiple places where the magnetic field is enhanced so that these are should carefully be designed and fabricated to suppress the excess magnetic field. The electric field may also be enhanced if any burrs and scratches exist on high electric field area. The care to be burr free, micro-protrusion free, and particle free on surface is also an issue to be considered not only the SCC cavity but also for NCC cavities.

10.3 Summary of LINAC-II

By keeping the emittance growth within a tolerable level, the luminosity will be kept high. Various sources, especially those of wake-field origin, were discussed. Then the cures of HOM origin are discussed in detail. Cares on alignment to suppress single-bunch wake field was discussed, using structure BPM and BBA.

These perturbations and cures are almost the same in general in both warm linac and cold one and should be carefully designed and realized to keep the high luminosity.

References

[1] A. W. Chao, "Physics of Collective Beam Instabilities in High Energy Accelerators," John Wiley & Sons, Inc., ISBN 0-471-55184-8, 1993.
[2] T. Weiland and R. Wanzenberg, "Wake fields and Impedances", DESY M-91-06, 1991.
[3] W. K. H. Panofsky and W. Wenzel, Rev. Sci. Instr. 27, 967, 1956.
[4] P. B. Wilson, "High Energy Electron Liancs: Application to Storage Ring RF System and Linear Collider," SLAC-PUB-2884, 1982.
[5] E. Keil, NIM 100, 419, 1972.
[6] K. Bane and B. Zotter, Computer code TRANSVRS, 11th Int. Conf. High Energy Accelerators, p581, Geneva, 1980.
[7] K. L. F. Bane, "Short-range dipole wakefields in accelerating structures for the NLC," SLAC-PUB-9663, 2003.
[8] A. W. Chao, B. Richter and C. Y. Yao, NIM, 178, p1, 1980.
[9] V. E. Balakin, A. V. Novokhatsky and V. P. Smirnov, Int. Conf. on High-Energy Accelerators, p119, 1983.
[10] G. V. Stupakov, "Physics and Technology of Linear Accelerator Systems," World Scientific Publishing Co., ISBN 981-238-463-4, Proc. 2002 Joint USPAS-CAS-Japan-Russia Accelerator School, California, 2002.
[11] E. Jensen, ibid.
[12] K. L. F. Bane and R. L. Gluckstern, "The Transverse Wakefield of a Detuned X-Band Accelerator Structure," SLAC-PUB-5783, 1992, and R. M. Jones, "Advanced Damped Detuned Structure Development at SLAC," PAC97, 1997.
[13] U. van Rienen, "Higher Order Mode Analysis of Tapered Disk-Loaded Waveguide using the Mode Matching Technique," Particle Accelerator, V41, p173, 1993.
[14] HFSS, http://www.ansoft.com
[15] K. Ko, "High Performance Computing in Accelerator Structure (RDDS1)," WE201, LINAC2000, Monterey, USA, 2000.
[16] MAFIA, http://www.cst.de
[17] GdfidL, http;//www.gdfidl.de
[18] M. Yamamoto, "Study of Long-Range Wake Field in Accelerating Structure of Linac," KEK Report 94-9, 1995.
[19] R. M. Jones, "A spectral Function Method Applied to the Calculation of the Wake Function for the NLCTA," SLAC-PUB-7287, 1996.
[20] "International Study Group Progress Report on Linear Collider Development," KEK-Report 2000-7.
[21] C. Adolphsen et al., "Measurement of Wake-Field Suppression in a Detuned X-Band Accelerator Structure," Physical Review Letters, vol27, p2475, 1995.
[22] T. Raubenheimer , NIM A306, p63,1991.
[23] R. H. Fowler and L. Northeim, Proc. Roy. Soc., A119, p173, 1928.
[24] J. Wang and G. Loew, SLAC-PUB-7684, and J. Wang, PhD thesis, Stanford University, SLAC-339, 1980.
[25] R. Helm and R. Miller, in Linear Accelerators, ed. by P. M. Lapostolle and A. L. Septier, North-Holland Publishing Co., 1970.
[26] D. P. Pritzkau, Thesis, p99, SLAC-Report 577.
[27] V. Dolgashev and L. Laurent, Advanced Accelerator Concept Workshop, AAS 2008, USA.